Available online at www.sciencedirect.com
ScienceDirect
Computers and Geotechnics 34 (2007) 306–327
COMPUTERS AND GEOTECHNICS
www.elsevier.com/locate/compgeo

Coupled chemo-mechanics of intergranular contact: Toward a three-scale model

Liang Bo Hu, Tomasz Hueckel *

Department of Civil and Environmental Engineering, Duke University, Durham, NC, USA

Available online 20 April 2007

Abstract

Mineral dissolution in the vicinity of a stressed grain contact undergoing irreversible damage strain is studied numerically at three scales: of a grain, grain assembly and macroscopic continuum. Rigid chemo-plasticity is used to simulate the phenomena in the solid phase at the micro-scale, coupled with the reactive-diffusion transport of the dissolved mineral across the grain. Dilatancy resulting from the material damage generates new free surface area around the asperity, in turn enhancing dissolution and material weakening. Extended Johnson approximation of the near-contact field is adopted. Upscaled variables at meso-scale simulate the stiffening of the grain system as a result of the subsequent mineral precipitation. The consequent redistribution of mass within the pore space, affecting soil porosity and stiffness is derived on macro-scale from the averaged micro-scale variables. Partial masses of the same mineral are shown to play different roles at macro-scale, which requires linking them to different processes (dissolution and precipitation) derivable only at a micro-scale. Cross-scale transfer formulation is investigated. The study applies to many processes of fluid–solid interdependence in soil mechanics, such as structuration and aging of natural soils, compaction and pressure solution of oil or gas bearing sediments.

Keywords: Grain contact; Chemo-plasticity; Chemo-mechanics; Coupled phenomena; Multi-scale; Dissolution; Precipitation; Aging; Pressure solution; Silica–water reaction

1. Introduction

Most of natural and engineering processes in mechanics of geomaterials involve intergranular forces and displacements, which at the continuum level are represented by stress and strain fields. A well developed continuum mechanics theory of granular medium would usually allow one to competently deal with most soil mechanics problems. However, as grain contact phenomena, especially for fluid saturated soils, are often substantially affected by mineral alterations at the micro-scale, purely mechanical considerations may not be sufficient over larger time scales. Such alterations are mainly due to chemical phenomena between solid and fluid phases and driven by chemical variables, which from the mechanics point of view, are internal variables and hence, uncontrollable. A better understanding of what mechanisms control the contact process at the micro-scale will allow us to more completely represent this process at the macroscopic scale.

Diverse processes in geomechanics are known to directly depend on the microscopic level dissolution of minerals at the stressed intergranular contact. They include: structuration or post-sedimentary development of a secondary micro-structure in natural soils, aging of materials in laboratory tests, intergranular cementation, and compaction of oil bearing sediments via induced pressure solution, as well as the degradation processes of weathering, micro-erosion, desiccation cracking, etc. While the time scale and contribution of different mechanisms constituting these processes may be different in each of the phenomena mentioned, one feature that these processes appear to have in common, is the redistribution of mass of solids within the soil. The specific mechanisms of this redistribution are a subject of a more or less intense debate in the respective communities and a subject of both theoretical and experimental

* Corresponding author. Tel.: +1 9196605205.
E-mail address: hueckel@duke.edu (T. Hueckel).

0266-352X/$ - see front matter © 2007 Elsevier Ltd. All rights reserved.
doi:10.1016/j.compgeo.2007.02.009

research. The redistribution is often linked to a series of processes such as dissolution of compounds and minerals, diffusion, formation of gel in pores, precipitation of mass on exposed (free) surfaces. It often produces changes in mechanical properties of material at a macro-scale. While some geochemical mechanisms of the above lists have been analyzed using micro-scale models, their outcome, such as alteration of the mechanical properties of material at a macro-scale is often unnoticed, with the exception of cementation effect.

In this paper, we further develop an earlier concept of coupled chemo-plasticity [1,2] by linking irreversible dilatancy and the increase of the free surface area to the increased dissolution of minerals per unit volume, enhancing in turn the chemical softening of the material [3].

It seems clear from the above considerations that the chemo-mechanical behavior of the grain assembly cannot be confidently dealt with at a single length scale only. While the ultimate scale and the corresponding variables are macroscopic and continual, phenomena that cause the involved processes and the corresponding variables are quantified at the (chemistry) molecular scale. To characterize the chemically induced changes in mechanical properties it may appear necessary to identify idealized meso-structures that undergo such an evolution and mechanisms determining the end result: variation in the continual material properties.

Therefore, in this paper for the particular scales we choose representative elementary volumes, which contain: for the micro-scale deformation and intra-granular transport: a microscopic continuum of the material of an individual grain encompassing a representative volume of micro-cracks of few tens of a micron; for the meso-scale inter-granular transport and deformability evolution of a grain system: a characteristic unit of four solid grains endowed with initially free surface of grains, on which precipitation occurs forming a thin coating, and the same unit surrounding an inter-grain pore and deforming around it as a hollow cylinder; for the macro-scale: a continuum of assemblies of grains characterized by a Cam-clay type chemo-plasticity.

At each scale the boundary value problems formulated is obviously different as they describe different mechanisms. An important part of such a multiple scale modeling is the cross-scale transfer functions. In this paper they are formulated for the macro-scale constitutive functions based on averaging of meso-scale and micro-scale variables of mass change of the same mineral but engaged in distinctly different lower-scale phenomena.

2. Macroscopic observations on soils exposed to aging

One of the areas, where a proper understanding of intergranular contact phenomena is crucial for the industrial decision-making is water, petroleum or methane gas extraction from underground reservoirs. A key element of this decision-making is the assessment of reservoir compaction and a potential for land subsidence. Especially in coastal areas, even a small amount of subsidence may cause flooding and severe damage to the urban infrastructures.

One of the principal factors of a fundamental relevance in the aging experiments is the post-aging increase in stiffness. Fig. 1 (from [4]) shows the essential features of the post-aging stress–strain response (A5) of clayey sand and sand sediments from Adriatic from the depth of 3270 m. In this test, compared to a regular oedometer test result (A4) from the same depth, the specimen was subjected to a 14 day-aging at a constant axial stress corresponding to the in situ stress (35.04 MPa). Both clayey sands and sandy clays, either undisturbed or remolded, at a high and a low stress level, with an organic matter present or not, exhibit the same behavior as known for some time (see e.g. [5,6]). They show a secondary compression (creep) strain (a–b in Fig. 1a) the amount of which depends on time and constant stress value. The post-aging stiffness is almost

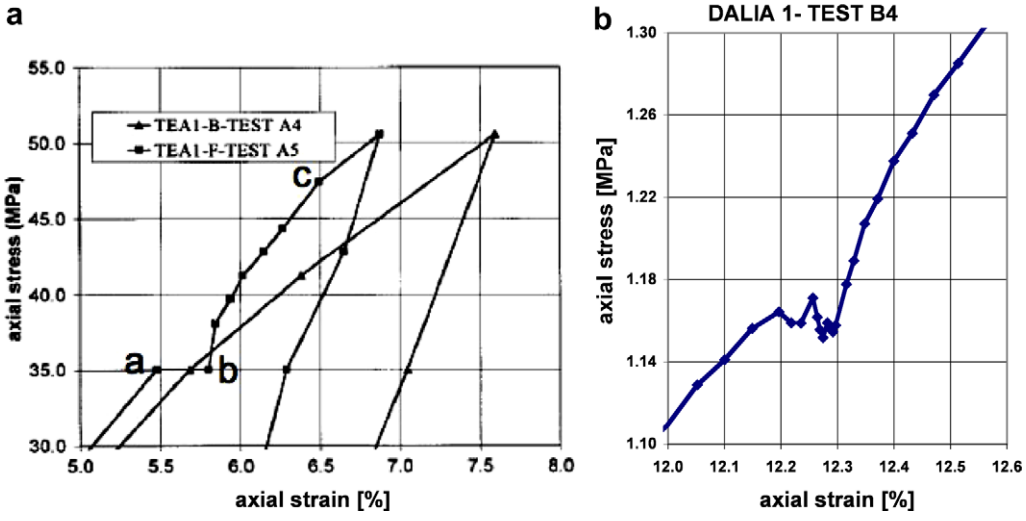

Fig. 1. Post-aging increased stiffness. (a) Comparison between oedometer test results with 14 day aging (A5) and without aging (A4) of the sample of Tea 1 sediment from 3270 m of depth. (b) The effect of $2\frac{1}{2}$ h aging on Dalia sand from 1200 m of depth.

twice as high as the pre-aging one, it is highly non-linear and tends to that of a non-aged specimen beyond certain stress threshold (marked c in Fig. 1a).

The post-aging stiffness is extremely important as it presumably represents the in situ stiffness. Hence, the stress threshold value that demarks an enhanced stiffness range is also very important. It appears that the threshold stress depends on the amount of the aging strain. The value of that stress range of enhanced stiffness may be represented by the threshold stress less the in situ stress, divided by the in situ stress. The experimental data presented in Fig. 1a are plotted in Fig. 2a against the axial secondary compression strain normalized with respect to the strain at the onset of aging.

It appears that the enhanced stiffness range does not grow beyond 15% of the in situ stress in the case of the tested sand, and we may expect that there are similar cut-off numbers for other soils. It is about twice as much for clayey Tea 1 sediment. The cut-off appeared increasing up to the accumulated aging strain about 4% of strain at the onset of aging. Interestingly the data did not seem to be correlated with the duration of the aging test. Early theories [7] suggested that the range ends when the post-aging curve meets an extension of the original normal consolidation stress–strain line. Experiments by Hueckel et al. [4] do not confirm that to be a rule, but it could be a convenient approximation.

Moreover, the rate of aging straining at the beginning quite high, around 10 h undergoes quite a change, dropping to a value about 10 times lower (Fig. 2b), and then remaining constant. It is interpreted that the first about 2800 min (20 h) is related to Darcian water removal from macro-pore, whereas the further process is linked to a time dependent solid mass redistribution.

As a current standard method to predict soil and sediment compaction is based on determination of 24-h soil compressibility in laboratory tests, such predictions invariably tend to overestimate the subsidence, compared to the values measured in situ. This difference is usually attributed to the fact that handling and unloading during the retrieving and transport causes certain damage to the samples, which thereafter appear more compressive in the testing. However, new aspects of this traditional explanation emerge in view of the testing technique allowing for a two-week aging under constant stress. The resulting compressibility appears to be much closer to the radioactive marker field data [8], suggesting an alternative interpretation [9]. It is now broadly accepted also in geotechnical testing that the difference between the soil response in the laboratory and the field comes from creep and aging that the latter soil underwent (see e.g. [10]).

3. Geochemical evidence of intergranular aging

The results obtained also indicate that the increase of the material stiffness is clearly a time dependent phenomenon [4]. However, they also suggest that the time scale of the underlying physico-chemical processes is that of week or months, rather than millennia or more. This latter observation differentiates them from the processes understood as pressure solution occurring over the geological ages. Both soil aging and pressure solution seem to encompass the evolution of physical and mechanical properties of soils during the long-term constant loading or secondary compression. The hypothetical microscopic mechanisms, following Mitchell and Solymar [11] and experiments by Denisov and Reltov [12], include the local dissolution/precipitation of some geochemically less stable minerals and formation of a secondary micro-structure. However, a most recent macro-scale investigation of aging throws more light on the phenomena involved. Baxter and Mitchell [13] confirmed a substantial dissolution of minerals within 3 months. However, they found no consistent evidence of any local precipitation.

Modeling of intergranular contact dissolution has a long history. Early hypotheses [14,15] included formation of a layer of adsorbed water, which serves as the conduit for the dissolved species. More elaborate developments of these models [16–18] focus on the mechanism of mass removal and transport in open or closed systems and have been associated with the process of pressure solution.

Pressure solution is defined as a deformation resulting from transfer of solid material from highly stressed areas through diffusion in pore solution toward stress-free areas

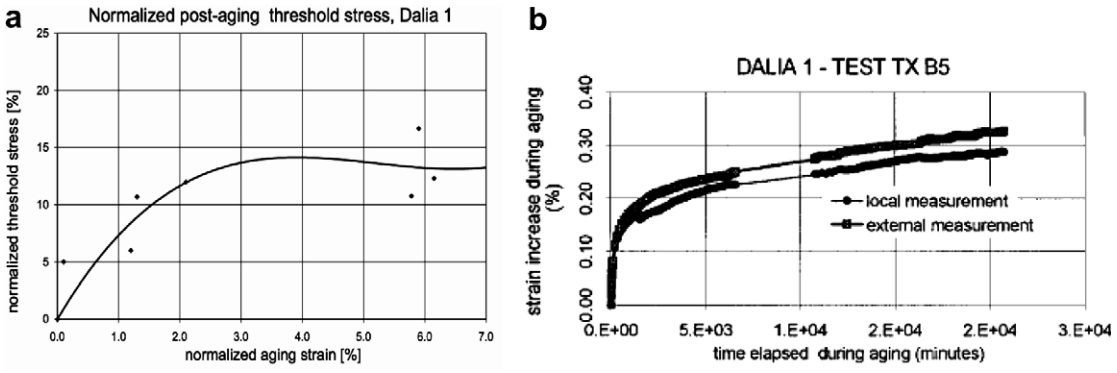

Fig. 2. (a) Normalized post-aging threshold stress of Dalia sand. (b) The evolution of aging strain on Dalia sand.

(driven by stress gradient), or from the areas with a higher chemical potential to those with a lower chemical potential (driven by chemical potential gradient). It is one of the main mechanisms for compaction, cementation and deformation of sedimentary rocks during diagenesis or medium grade metamorphism [19,15,20,21]. The emphasis in pressure solution studies is almost entirely on reduction of porosity [18].

The process of pressure solution is explained via several mechanisms, which are either sequential or parallel. It is possible that different scenarios are more pertinent for different minerals, and that some of their elements occur simultaneously with different intensities. Among mechanisms proposed for the elementary process of pressure solution, the water film diffusion and free-face pressure solution are particularly favored by geochemists. The former assumes that dissolution takes place at the grain contact area with solutes diffusing along an adsorbed water film layer [14,15]. Alternatively, a so-called ''island–channel'' structure etched chemically in the mineral may provide access to dissolution sites as well as a preferential path of transport of solute [22,23]. Another major issue in debate is the driving force of pressure solution. It was early proposed that the differential stress (stress gradient) in the solids controls the mass transport [24,25]; later the chemical potential gradient became widely accepted as the driving force. The chemical potential is a rate with which internal energy increases as a result of addition of mass (number of mols at constant volume) to the system. The questions, how this potential should be formed, and with which stress the chemical potential should be associated, are a subject of debate. A model with chemical potential gradient as a driving force linking the mechanics (usually the stress) to chemistry (kinetics) has been proposed by Dewers and Ortoleva [26].

The mechanics of the neighborhood of the contact is considered to be in the elastic domain [18,27]. However, even if the evidence pointing to a role of micro-cracking in the vicinity of contact is now overwhelming (see Section 4), modeling of damage or other forms of irreversible deformation in the dissolution affected zone has not been pursued with a similar success. This is despite of early indications of dissolution occurring along micro-cracks at grain contacts [28]. Stressed contact phenomena have also been studied in powders and ceramic media (see e.g. [29,30]). Subramonian and Sofronis [27] suggest that the diffusion takes place along the grain interface and that there is a mass flux originally from the free grain surface driven by the surface curvature. Finally, there is a scenario which suggests that mechanical deformation, particularly plastic deformation or micro-fractures may play an important role in the process of pressure solution [31,32].

Near-contact damage and irreversible deformation were observed during pressure solution studies in a number of studies. Their effects on the dissolution are also recognized and include the following aspects: (1) the micro-fractures generated by damage or plastic deformation enhance the solubility at contact zone [33–35,31,32]. (2) Deformed material is extruded and then exposed as a free surface and subsequently dissolved [32].

Ostapenko's work [33,34] emphasized the role of plastic deformation in enhancing fluid percolation and increasing the solubility at contact zone. Pharr and Ashby [36] believe that a neck between grains grows by plastic deformation and proposed a coupled plasticity-and-dissolution model. An experimental study of knife-edge pressure solution of halite conducted by Tada and Siever [31] convinced these authors that pressure solution is most likely a mechanism combining plastic deformation and free-face pressure dissolution [32]. Near-contact cracking has also been seen by Milliken [37] and Dewers and Hajash [38]. Gratz [39] considers micro-cracks at contacts as a primary mechanism of pressure solution. He envisioned that they actually evolve into the channel-and-island structures and provide a plumbing system for the transport of the dissolved material from their walls. den Brok [40] provided an experimental evidence to support Gratz's model (see also [41]). Hickman and Evans [42] observed a typical elasto-plastic yielding of the contact concomitant with a high dislocation density. Recent observations of indentation of silica grains at a nanoscale show an advanced damage of the contact area and a visible creep [43].

The scenarios that will be examined in this paper are limited to those that involve coupling between the deformation and damage of the solid grains and dissolution of the mineral mass enhanced by that damage. It must be underlined that the scenarios proposed in what follows represent one of several possible options that could be considered. Only a comparative assessment of several such options against physical evidence will yield a comprehensive picture of the phenomena involved.

In this paper, a consistent microscopic scenario of the intergranular contact will be developed with the emphasis on a novel concept of damage enhancing dissolution. The underlying mechanisms of these processes include plasticity coupled with a linear reactive diffusion to provide a quantitative assessment of the micro-scale phenomena.

4. Microscopic scenarios of a submerged intergranular contact process

A series of qualitative experiments using chalk bars immersed in a light salt solution were performed [44], visualizing the chemically enhanced damage. Identical chalk bars were used with fluid of different salinities or without fluid. Indentation was conducted using metal indenter, wooden indenter and chalk-to-chalk indentation. Chalk was selected as a modeling material for two reasons: a high rate of reaction; and a good representation of the brittle behavior, typical of silica or calcite. The following observations are made: (1) with all types of indenters, there is a visible damage of the material at the contact. (2) mass under the metal indenter in high salinity (Fig. 3) is removed much faster from the damaged zone, compared to the tests on the

chalk bars in a lower salinity fluid or without water. (3) Figs. 4 and 5 show the same tests after 24 h and 64 h. There is a significant progress of damage between 24th and 64th hour, also, more material is precipitated underneath under the latter time. (4) Fig. 6 shows the top view of the damaged contact area under metal indenter. There are visible damaged chalk pieces in the contact range proving the existence of newly generated free surfaces. Small craters are formed by a reaction producing gas at the free surface around as well as within the damaged zone.

The presence of an enhanced damage by solid–fluid interaction are observed in other mineral as well ([45], Fig. 7). The following scenario for a coupled damage and dissolution at intergranular contact is proposed. The area under consideration is the immediate vicinity of the stressed grain contact immersed in macro-pore water. The pore water is assumed to drain freely, generating no pore pressure. It is assumed that the load is sufficient for yielding (involving damage) to occur in that area. The damage is quantified in terms of an irreversible dilatant strain associated with an increase in the specific surface area through newly generated micro-cracks. Dilatancy at micro-sub-granular-scale sucks water under a negative pressure into a micro-cracked damage zone. Furthermore, as the reaction rate of any dissolution is proportional to the surface area of the reaction, it follows that the reaction rate is coupled to the irreversible deformation. On the other hand the removal of mass of silica from the material at the grain scale via reaction causes the material softening at the larger scale. Fig. 8 presents a cartoon of the phenomena involved. To compensate for the strength loss at a constant stress, plastic strain hardening arises in the material.

Fig. 6. Top view of damaged contact area.

Fig. 3. Edge penetration into chalks submerged in the salt water.

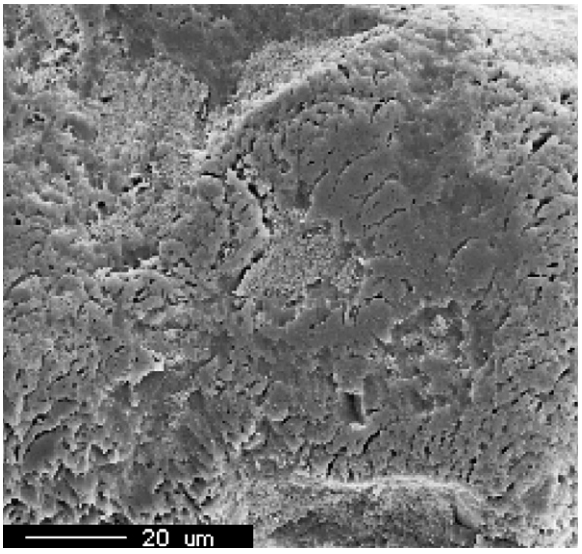

Fig. 7. SEM photography which shows the dissolution spots at grain contacts of St. Peter quartz sand subjected to 150 °C and 34.5 MPa of effective pressure for about 14 months (reproduced from [45], by permission of Am. J. Sci).

Fig. 4. Dissolution and damage at the chalk contact after 24 h.

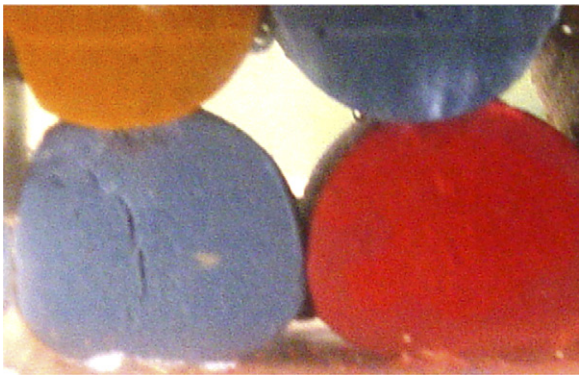

Fig. 5. Dissolution and damage at the chalk contact after 64 h.

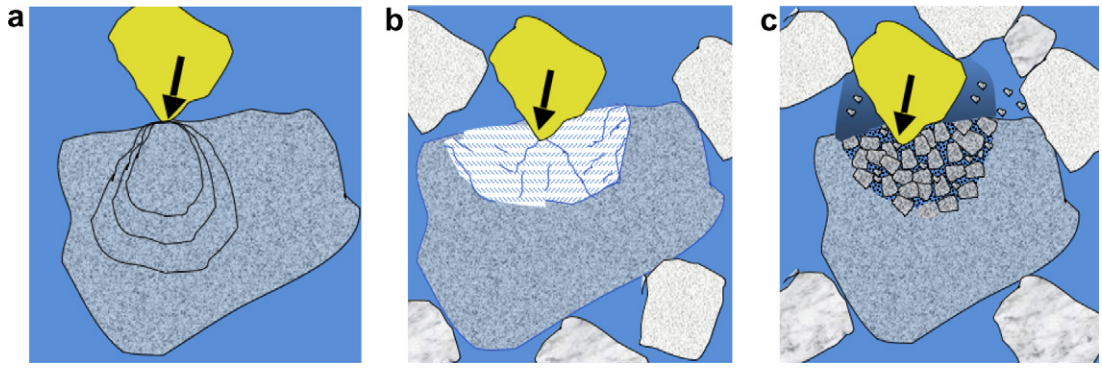

Fig. 8. A cartoon showing a process of indentation of a rigid grain into a deformable grain: (a) elastic phase: isobars; (b) plastic phase: a plastic zone characterized by micro-cracking and dilatancy; (c) chemo-plastic phase: removal of mineral mass from dissolving surfaces and progressing cracking of the medium.

Hence, the plastic behavior is a combination of strain hardening and chemically controlled mass removal softening.

Dissolution increases the concentration of the product species in the micro-pore interstitial water in the damaged zone, which generates a gradient of concentration with respect to the grain boundary. The gradient causes a short-range transport of the solutes within the grain towards its boundary and the flux into the macro-pore water. The final part of this scenario consists of the fate of the solute, which is its mid- to long-range transport, possible precipitation and related strength increase effects. A classical scenario of coating of free grain surface with precipitates with a mid-range, inside of macro-pore transport will be considered. The mechanical deformation is considered as instantaneous, while dissolution is time rate dependent. A general formulation for this type of model has been presented by Hu and Hueckel [46].

5. Micro-scale model for the coupled damage – dissolution–diffusion

The question at hand is: what is the effect that the irreversible damage developed at an intergranular contact may have on dissolution of minerals from the damage area, and vice versa, what is the effect of mineral dissolution on the strength reduction and hence further mechanical damage, but also on a macro-void filling via long range precipitation and the resulting strength increase at the macro-scale? We consider indentation of a harder (undeformable) grain into a (softer) grain of quartz supported by an external load over an undefined period of time. Water may infiltrate into the grain as it undergoes micro-cracking. The grain is part of a water-saturated assembly. The mechanical processes are considered instantaneous, unless conditioned by the time scale of chemical reactions. Water permeation is also considered as instantaneous compared to the reaction time.

5.1. Conceptual constitutive modeling

Mathematical formulation of the above outlined scenario requires a series of constitutive hypotheses and specific assumptions concerning the mechanisms of the chemo-mechanical coupling. These hypotheses address mechanics of the material deformation and damage, chemical reactions, chemical transport, and finally the forms of coupling.

For that purpose we shall develop further an earlier idea that a mass removed from/added to a solid isochorically (without the volume change of the representative elementary volume of the porous medium) and adiabatically (without heat exchange) affects both the medium compliance and strength [1,2,44,46]. These two mechanical properties will be addressed in the framework of reactive chemo-plasticity. This term is used as opposed to non-reactive chemo-plasticity [47], taking place when a change in concentration (of selected species) of pore fluid produces an instantaneous change in mechanical properties of the solid fraction and of soil *per se*. Reactive and non-reactive chemo-plasticity are distinguished in analogy to reactive and non-reactive transport. The importance of this distinction results from a difference in *time scales*, which are either that of kinetic processes or diffusive–advective processes, correspondingly.

It is visible from the schematization in Fig. 8 that the problem needs to be treated also at several (three) *geometrical scales*. It has to be clear when discussing material properties and assumptions about the system, at what scale these properties need to be measured. At macroscopic scale the soil is assumed to be a two-phase multi-component (minerals) porous material, saturated with water. A representative elementary volume (REV) of the porous medium, with the two phases superimposed, is represented by a single geometrical point, to which all the mechanical and chemical properties are attributed. Hence, the properties of the solid phase need to include the presence of macro-voids and intergranular, or meso-pores and the effects of intergranular friction. Clearly, a REV size must be such to include a sufficient number of grains, pores and intergranular contacts. In other words, a REV for macro-continuum is deemed to contain an assembly at least 10 times larger than that in Fig. 8b or c.

A more specific assumption made for the purpose of this particular problem requires that the processes involved at that scale are sufficiently slow for the material to be considered as perfectly drained and consequently, the fluid phase as carrying no partial stress.

The phenomena we intend to focus on in what follows have their origin and governing gradients occurring at a smaller scale, to which we will refer as a micro-scale. The medium considered is that ***within*** a single soil grain. A REV at the micro-scale must contain micro-cracks (typically of 10 μm in length, see e.g. [32]) sufficient in number (tens to a hundred of them) to form a continuum. While we do not intend to describe discrete discontinuities and rock fragments, nor their surfaces individually, we do account for their presence and role by including some of the relevant information quantified at a lower, molecular scale. The micro-scale is the main scale of our interest. The material properties at this scale are those of the grain rock including its porosity, micro-dilatancy, permeability and mineral composition. Specific assumptions for this scale include the postulate that the solid phase material is rigid-plastic, with the understanding that a sufficient load is applied to induce initial yielding, at least.

The chemical reactions are taken into account also at the micro-scale. The quantities being considered are moles of individual chemical or mineral components, or their masses (molecular scale). Chemistry describes, among others, dissolution of minerals from the wall surface of a micro-crack. The size of the representative elementary volume is such that contains a sufficient number of such micro-cracks and hence of the dissolution sites per unit volume, and hence is sufficient to be considered to be continuum. It is assumed that dissolution and local precipitation does not need to occur within the same crack but within the REV. However, the mid-range transport, or physically outside of the grain, but in the adjacent meso-pore space, as well as the long range transport outside REV are imaginable in the present context. The meso-scale includes the pores between the grains which are essential for the question of stability of the medium.

An important component of this type of modeling activity is an inter-scaling of variables. As will be seen, chemical (molecular) variables will need to be represented at the micro-scale, to represent molecular scale processes (dissolution) that affect properties exclusively formulated at macro-scale, such as hardening or yield limit expressed via strain or stress.

5.2. Micro-scale coupled chemo-plasticity model

As mentioned earlier the medium at this scale is the porous material that constitutes the solid grains of rock. Its porosity is the internal grain porosity, and the mechanical properties of the material are those of the grain rock.

The material of individual grain is approximated by the assumption of rigid-plasticity. This is to say that there is no strain (ε_{ij}) for a stress σ_{ij} within the yield locus, $f(\sigma_{ij}) < 0$, whereas at yielding, the strain rate is entirely irreversible, hence

$$\begin{aligned} &\text{if } f < 0, \text{ or } f = 0,\ \dot{f} < 0; \quad \dot{\varepsilon}_{ij} = 0; \\ &\text{if } f(\sigma_{ij}, p_c) = 0 \text{ and } \dot{f}(\dot{\sigma}_{ij}, \dot{p}_c) = 0; \quad \dot{\varepsilon}_{kl} = \dot{\varepsilon}^{\text{irr}}_{kl} \neq 0 \end{aligned} \tag{1}$$

Stress and strain are micro-stresses and micro-strains at the scale of a fraction of the grain. Stress and strain are considered as positive when compressive. Strains are assumed to be small. The superimposed dot over a symbol denotes a time rate.

A central role in the chosen form of the chemo-mechanical coupling is played by a dilatancy-damage phenomenon that occurs in some conditions during yielding. It is implicitly linked to micro-cracking. Micro-crack walls produce new solid–fluid interfaces, which constitute a source of dissolution of mineral species, which is a form of the solid mass removal. As a result of that, the yielding behavior of the material is affected by two competing plastic hardening mechanisms: deviatoric strain-hardening and mass removal softening. Hence, p_c, which is an isotropic size characteristics of the yield locus, depends on a set of hardening parameters, that are either mechanical ($\varepsilon^{\text{irr}}_q$) or chemical ($\xi$) in nature [1,2].

$$p_c = p_c(\varepsilon^{\text{irr}}_q, \xi) \tag{2}$$

In a sense this assumption reflects two different and independent ways in which the material may become harder or softer. One is a classical deviatoric strain hardening and the other reflects the strain-unrelated removal of mass role in weakening of the material. It is important to note that while later on we will postulate that mass removal is coupled to strain, it is not a necessary assumption.

The deviatoric strain hardening parameter $\varepsilon^{\text{irr}}_q$ is assumed as always positive and defined as

$$\dot{\varepsilon}^{\text{irr}}_q = \left(\frac{2}{3}\dot{e}^{\text{irr}}_{ij}\dot{e}^{\text{irr}}_{ij}\right)^{1/2}, \quad \text{where } \dot{e}^{\text{irr}}_{ij} = \dot{\varepsilon}^{\text{irr}}_{ij} - \frac{1}{3}\dot{\varepsilon}^{\text{irr}}_{kk}\delta_{ij} \tag{3}$$

Chemical softening parameter ξ represents accumulated relative mass removal/addition of a particular mineral species that predominantly contributes to the material strength or yield limit. It is calculated with respect to the original total mass of that particular species. The rate of removal is calculated from the rate of kinetic reaction. In principle, more than one reaction or process, may affect the strength of any geomaterial. These processes may be simultaneous or sequential, and each with a possibly different rate. There is currently no widely accepted approach to the question how to identify and quantify contributions of mineral ingredient to the overall geomaterial strength or compressibility. Averaging, or homogenization techniques do not yield realistic outcomes as yet. Also, configuration aspects of particular species within the volume may play a critical role, like that of calcium carbonate at the bridges between silica grains. However, in some circumstances, a phenomenological relationship between strength and a reaction progress variable may be established empirically.

In what follows we will address a single reaction effect only, with a single rate.

Dissolution is characterized as a kinetic process with the dissolution rate proportional to the specific surface area of the newly generated interfaces. As the latter in turn depends on the dilatancy-damage, the strain hardening and chemical softening mechanism become coupled.

A main reaction occurring at the intergranular contact with a quartz grain is dissolution of silica in water described as

$$SiO_2(s) + 2H_2O(l) \leftrightarrow H_4SiO_4(aq) \tag{4}$$

As a result of dissolution of silica, a silicic acid (known also as aqueous silica), H_4SiO_4 is formed in aqueous solution, the concentration of which can easily be measured in water in direct contact with the dissolving surface. The rate of dissolution of quartz has been determined experimentally by Rimstidt and Barnes [48]. They directly measured the mass of silicic acid in an aqueous solution in an experiment in a closed environment, under the assumption that the interfacial area between the phases remained the same in the case of dissolution and precipitation. They concluded that the mass dissolved is proportional to the surface area of the interface between the two phases. For a system which contains mass of water $M_f = M_f^0 = 1$ kg, the fluid/solid interface surface area, A, is normalized with respect to $A^0 = 1\ m^2$ to yield a non-dimensional quantity $\widetilde{A} = \frac{A/A^0}{M_f/M_f^0}$. The mass loss of silica from the solid phase is expressed via activity (mass) of silicic acid, H_4SiO_4, dissolved in water. This is expressed via a rate equation for silica interaction with water, first established by Rimstidt and Barnes [48]:

$$\frac{da_{H_4SiO_4}}{dt} = \widetilde{A}\gamma_{H_4SiO_4}(k_+ a_{SiO_2} a_{H_2O}^2 - k_- a_{H_4SiO_4}) \tag{5}$$

where a_i are activities, and γ_i, activity coefficients, of ith species, while k_+ and k_- are rate constants of respectively forward and backward reactions. $\widetilde{A}$ is a dimensionless specific interfacial surface area, defined as above. As the number of moles of silicic acid produced is equal to that of silica removed from the solid, in what follows the rate of change of activity of silicic acid in pore water is used to calculate the rate of relative mass removal of silica, hence

$$\dot{\xi} = s\frac{da_{H_4SiO_4}}{dt}, \quad s = \frac{N_{H_2O}^0}{N_{SiO_2}^0} \tag{6}$$

where s is a ratio between the number of moles of water, $N_{H_2O}^0$ and silica, $N_{SiO_2}^0$ in the initial volume of the grain (see [46]). Having normalized the above rate using ratio s, ξ becomes constrained by the inequalities: $0 \leqslant \xi \leqslant 1$, and hence can be treated as reaction progress variable, as proposed by De Groot [49]. When $\xi = 1$, the reaction is completed, that is all silica is removed from the material.

We will adopt the idea previously developed at the macro-scale by Hu and Hueckel [46] of an increased dissolution, taking place due to creation of a new internal surface area of solid/fluid interface generated by the local damage. In the current context the damage occurs within a single grain and consists in opening of micro-cracks. The walls of the micro-cracks are sites of additional dissolution, causing an intense mass redistribution, and hence ulterior softening of the grain material. A scalar hidden variable is introduced representing the amount of the added surface area, $\tilde{a}$ normalized with respect to a unit area of 1 m^2, in a grain solid volume normalized with respect to 1 m^3. The total surface area of micro-cracks can be measured directly in experiments, as it is proportional to the total acoustic energy released during cracking and measured by acoustic emission. Variable $\tilde{a}$ needs to be linked to the relative reaction area, $\widetilde{A}$, as formulated in Rimstidt and Barnes [48], Eq. (5), and hence related to the volume of water with which the solid is reacting. Hence, a conversion factor is applied

$$\tilde{a} = \frac{A/A^0}{V/V^0} = \widetilde{A}\frac{n_g \rho_w}{\rho^0} \tag{7}$$

where $\rho^0 = 1$ kg/m^3, ρ_w is the density of water, n_g is porosity of the grain solid.

The cumulative frequency of acoustic emission events is known to be proportional to the inelastic dilatant volumetric strain [50,51]. The new internal interface surface area generated by the micro-cracking per unit volume of the medium has been assessed using a single model of a two-dimensional hexagonal crystal assembly [46]. It is proposed to be proportional to the volumetric strain, ε_v^{irr}, and inversely to an average crack opening at the apex, δ, considered as a rock characteristics (see e.g. Fig. 9)

$$\tilde{a} = 8/(\sqrt{3}\delta)|\varepsilon_v^{irr}| \cdot 1\ \text{m}, \quad \text{if } \varepsilon_v^{irr} < 0 \tag{8}$$

Hence,

$$\widetilde{A} = f(\varepsilon_v^{irr}) = \phi|\varepsilon_v| + \phi_c; \quad \varepsilon_v < 0 \tag{9a}$$

$$\varepsilon_v > 0; \quad \phi = 0 \tag{9b}$$

where ϕ is a proportionality constant, whereas ϕ_c represents the specific surface area of pre-existing voids per unit volume. The former inequality restricts the range of validity of the expression for the specific surface area to the dilatancy strain only. The latter inequality aims at excluding compressive volumetric strain. When the volumetric strain is compressive, there are no micro-cracks, hence it

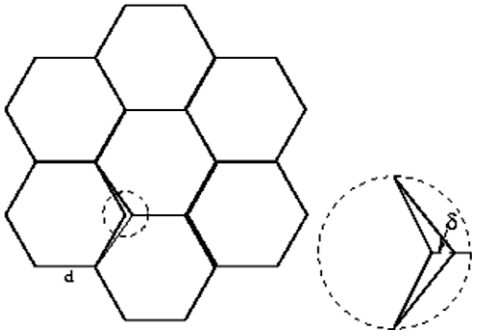

Fig. 9. Interfacial free surface generation within crystalline assembly.

is assumed that the dissolution surface area remains constant. In practice, without knowing the strain history or chemical reaction history of the system, it is convenient to set-up the initial time $t = 0$ as the moment at which the strain starts to develop, and assume that chemical reaction effect is disregarded before this time. The accumulated volumetric strain is zero before this time, while the above dissolution rate equation is not activated until the yielding takes place at $t \geqslant 0$.

The irreversible strain rate is determined by the associated flow rule according to which the strain rate mode is determined by the yield locus gradient, while the amount of the strain rate is controlled by the rate of change of plastic multiplier, $\dot{\Lambda}$

$$\dot{\varepsilon}_{ij}^{\mathrm{irr}} = \dot{\Lambda}\frac{\partial f}{\partial \sigma_{ij}} \tag{10}$$

Multiplier $\dot{\Lambda}$ is determined from the extended Prager's consistency condition, $\dot{f}(\sigma_{ij}, \varepsilon_q^{\mathrm{irr}}, \xi) = 0$ (see e.g. [52,2]) as a function of rates of stress and reaction progress

$$\dot{\Lambda} = \frac{\frac{\partial f}{\partial \sigma_{mn}}\dot{\sigma}_{mn} + \frac{\partial f}{\partial \xi}\dot{\xi}}{-\frac{\partial f}{\partial \varepsilon_q^{\mathrm{irr}}}\left[\frac{2}{3}\frac{\partial f}{\partial s_{ij}}\frac{\partial f}{\partial s_{ij}}\right]^{1/2}}; \quad \dot{\Lambda} = 0 \text{ if } f < 0 \text{ or } f = 0 \text{ and } \dot{f} < 0 \tag{11}$$

while $s_{ij} = \sigma_{ij} - \frac{1}{3}\sigma_{kk}\delta_{ij}$ is stress deviator.

5.3. Formulation of the coupled indentation-transport problem

To simulate deformation and mass flux generation at an intergranular contact the following approximate boundary value problem is formulated capturing hopefully the essential mechanisms involved. We consider a system of rigid-plastic grains of diversified yield limits (Fig. 10). An intergranular contact is represented by a penetration of a rigid asperity of a grain into the surface of another grain already in plastic state. It should be pointed out that many types of configurations of intergranular contacts within the grain system are possible. However, we restrict ourselves to the case when the material is under high stress and the indentation of asperities of grains into other grains becomes a dominant mechanism. Notably, a relatively flat contact surface may possibly contain multiple minor asperities, each of which could be modeled as an indenter. Note furthermore, that the shape of the indenter is of no great importance in the modeling, as will be seen later.

We consider an indentation of a frictionless asperity into a planar surface in plane strain state. The goal is to simulate the process of chemo-mechanical coupling in a zone immediately adjacent to the contact. We furthermore assume that this zone is not directly affected by any other contacts of the grain (Fig. 10). In fact, we shall assume that stress at the other boundary of the zone is comparatively small as the forces at other contacts are only a fraction of the indenting (or damaging) contact force, and hence the material at the other contacts remains rigid.

The formulation adopted is an extension of Johnson's approximation, well known in contact mechanics [53,54]. We choose to use a plane strain approximation of contacts between "cylindrical grains", rather than "spherical grains" for the relative analytical simplicity and for a possibility of prospective experimental verification. Accordingly, the contact surface of the indenter is assumed to be encased in a hemi-cylindrical "core" of radius a, within which stress is assumed to be a hydrostatic pressure p (Fig. 11). As Johnson pointed out, indentation experiments show that the stresses and strains are distributed nearly radially around the indentation point. Therefore, outside this core it could be assumed that the stresses, strains and displacements are axially symmetric and the same as in a rigid-plastic thick-walled cylinder with a, b as the inner and outer radius, respectively.

Stress boundary conditions apply at $r = a$ and $r = b$, while the lateral constraints are ignored. At the inner boundary $r = a$, only hydrostatic pressure is considered, hence there is no friction at the contact. Clearly, a is of the order of the radius of contact area and b is of the order of, but certainly less than, the grain radius. The hydrostatic pressure p can be considered as a local indentation pressure during loading.

The objective in this section is to find a relationship between the deformation due to indentation under a constant hydrostatic pressure on one side, and ensuing damage and dissolution of the material at inter-phase interfaces as

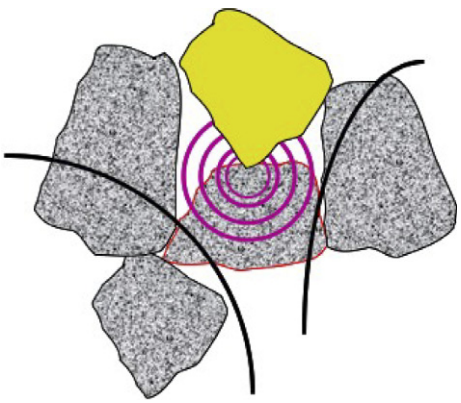

Fig. 10. Intergranular contacts in grain assembly.

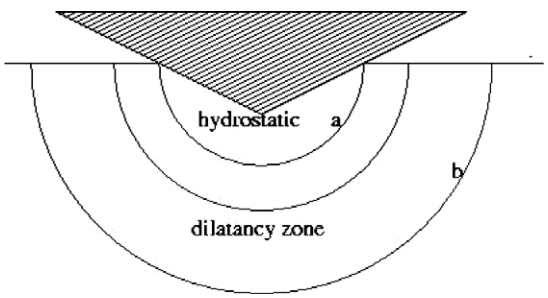

Fig. 11. Indentation model.

well as a mass flux generated through this process, on the other one.

In this development it is more important to replicate the physical and chemical mechanisms and their coupling, than to reproduce exactly the geometrical and boundary conditions. For this reason, intentionally, geometry, boundary conditions and constitutive functions were chosen as very simple. In particular, note that physical boundary conditions at the free surface of the grain, in particular traction conditions are intentionally not satisfied.

The reactive-diffusion process is idealized as follows. The grain has an initial interconnected porosity, mainly at inter-crystalline boundaries, which provides a pathway for a spontaneous diffusion in solution. This diffusion is maintained at a reference steady-state due to a background dissolution–precipitation. However, the dissolution–precipitation process in unstressed and/or in elastic conditions, possibly resulting in a Navarro – type of creep is not taken into the consideration. Our main interest is to study the phase in which inelastic deformation takes place, dissolution starts from micro-cracks (reproduced in this model by the irreversible dilatant strain), which generate a new specific free surface area of interface between solid and fluid phases. For the reason that our medium is assumed to be rigid-plastic, any pre-plastic process, including the effect of a prior mass removal from pre-existent pore walls is neglected, as it is a part of the material history that pre-dates our initial conditions. The onset of dissolution is induced by the onset of micro-cracking. This is reflected by the condition (9b). However, for the reason of the mass balance, the mineral production from the surfaces of the pre-existing pores is accounted for by the presence of ϕ_c in the expression for $\widetilde{A}$, see (9a).

The mathematical formulation of the BVP adopted is an extension of a plane strain problem externally pressured thick-walled cylinder formulated by Hill [55] and investigated by Mróz and Kwaszczynska [56] and Hueckel and Mróz [57]. These solutions will be extended to chemo-mechanical couplings.

5.4. Governing equations of coupled damage-dissolution and numerical simulation of the processes

A macro-scale problem of an internally pressured thick cylinder under spontaneous mineral dissolution has been discussed by Hu and Hueckel [46]. The current solution differs in the boundary conditions set-up to simulate the state of micro-stress in grain indentation, and in the loading program.

The stress boundary conditions are as follows (Fig. 12):

$$\text{at } r = a,\ \ \sigma_r = p_a; \quad \text{at } r = b,\ \ \sigma_r = 0 \tag{12}$$

As discussed earlier the zero normal traction at the outer boundary condition simulates a point-wise loaded grain supported at the other end by several other grains. We assume that the proportions between the grain size and asperity (indenter) size is greater than 10. Hence, the stress

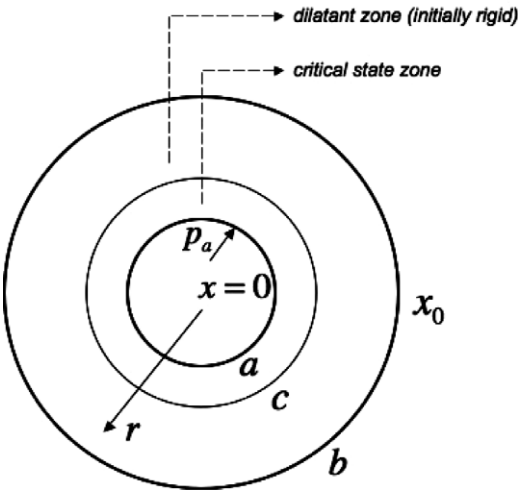

Fig. 12. Boundary conditions.

at the $r = b$, is assumed as uniformly distributed and small enough to be neglected, b being an artificial boundary in Johnson's approximation, deep enough into the grain. The global equilibrium of the grain is not of concern here, while it is satisfied for the axisymmetric problem being solved, analogously to the original Johnson's approximation.

The equilibrium equation and kinematic relationships for the plane strain axisymmetric problem are as follows:

$$\frac{\mathrm{d}\sigma_r}{\mathrm{d}r} + \frac{\sigma_r - \sigma_\theta}{r} = 0, \quad \dot{\varepsilon}_r = -\frac{\mathrm{d}\dot{u}}{\mathrm{d}r}, \quad \dot{\varepsilon}_\theta = -\frac{\dot{u}}{r} \tag{13}$$

where r, θ are outward radial and circumferential coordinates, respectively, u is a radial displacement. For the sake of simplicity, the yield limit will be taken as piecewise linear in the principal stress space, see Fig. 13:

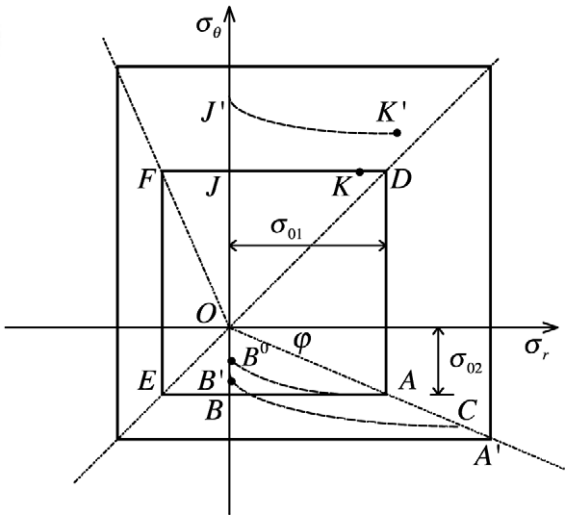

Fig. 13. Yield condition and stress profiles.

$$\begin{aligned}
&\text{for } \sigma_r<0;\ \sigma_\theta<0, \quad f=\sigma_\theta-\sigma_{02}=0, \ \text{or } f=\sigma_r-\sigma_{02}=0\\
&\text{for } \sigma_r<0;\ \sigma_\theta>0, \quad f=\sigma_\theta-\sigma_{01}=0, \ \text{or } f=\sigma_r-\sigma_{02}=0\\
&\text{for } \sigma_r>0;\ \sigma_\theta>0, \quad f=\sigma_\theta-\sigma_{01}=0, \ \text{or } f=\sigma_r-\sigma_{01}=0\\
&\text{for } \sigma_r>0;\ \sigma_\theta<0, \quad f=\sigma_\theta-\sigma_{02}=0, \ \text{or } f=\sigma_r-\sigma_{01}=0
\end{aligned} \tag{14}$$

The advantage of such locus is that when an associated flow rule is assumed, the kinematics is very simple, but capturing the essence of straining. The hardening rules are assumed as linear

$$\begin{aligned}
&\frac{\sigma_r}{\sigma_{01}}=1+\alpha\varepsilon_q-\beta\xi\geqslant 0,\\
&\frac{\sigma_\theta}{\sigma_{02}}=1+\alpha\varepsilon_q-\beta\xi\geqslant 0; \quad \sigma_{01}\geqslant 0;\ \sigma_{02}\leqslant 0
\end{aligned} \tag{15}$$

where α and β are respectively strain hardening and chemical weakening material constants, taken here for simplicity the same for σ_r and σ_θ. ε_q is deviatoric strain and defined as $\varepsilon_q=|\varepsilon_\theta-\varepsilon_r|$. σ_z remains undetermined. As discussed earlier, ξ is the relative mass removal, as its rate is described by Eq. (6). At this point the precipitation term is ignored as it would lead to a constitutive non-linearity, making it impossible to solve the equation system semi-analytically. Hence,

$$\dot{\xi}=A_{\mathrm{d}}s\gamma_{\mathrm{H_4SiO_4}}k_+a_{\mathrm{SiO_2}}a_{\mathrm{H_2O}}^2, \quad A_{\mathrm{d}}=\phi|\varepsilon_{\mathrm{v}}|+\text{const}; \ \ \varepsilon_{\mathrm{v}}<0 \tag{16}$$

The activities are assumed to be unities. ξ in the simulation becomes

$$\dot{\xi}=k_+(\Xi\varepsilon_{\mathrm{v}}+\Xi_0), \ \ \Xi=s\phi, \ \ \Xi_0=\text{const}; \quad 0\leqslant\xi\leqslant 1 \tag{17}$$

Ξ_0 is a constant related to the surface area of the initial micro-pore. $\gamma_{\mathrm{H_4SiO_4}}=1$; $a_{\mathrm{SiO_2}}=1$ and $a_{\mathrm{H_2O}}=1$. Notably, Eq. (17) appears now dependent on a deformational variable and on none of the chemical ones, and time. Given the linearity of the theory as presented, the integrated mass removal ξ is a linear function of time. When ξ reaches 1, the whole mass fraction of silica is removed from the material and the reaction is completed. Including a local precipitation in this model is feasible, as shown in Hu and Hueckel [46], but requires a non-linear formulation.

It should also be noted that the choice of a deviatoric strain hardening function in Eq. (2) is of a particular consequence. As shown by Hu and Hueckel [46], to allow a chemically induced irreversible strain at a constant stress, a compensation mode is induced between the two hardening terms, if $\varepsilon_q^{\mathrm{irr}}>0$ and $\xi>0$. Note, that requirement of the compensation mode limits the use of the classical volumetric strain softening function instead of deviatoric strain hardening. Both functions are commonly used in the dilatant regime of geomaterials. However, as demonstrated by Hu [44], the employment of volumetric strain softening leads to a possible instable behavior of the material and may imply a loss of stability of granular force chains due to chemical reactions, the occurrence that is observed in granular systems [58].

The process considered is composed of two phases. An initial phase corresponds to a grain point load equivalent to reaching the in situ loading. It consists in an increasing loading at the inner boundary $r=a$ up to value $\sigma_{ra}=p_a$ ($p_a>\sigma_{01}$). Before the inner load reaches the initial yield stress σ_{01}, the whole grain remains rigid. Once σ_{01} is exceeded at $r=a$, an inner plastic zone develops between $r=a$ and a certain radius $r=c$. The radial stress at $r=a$ is represented in the stress space in Fig. 13 as a point moving along the critical line AA', from A ($\sigma_{ra}=\sigma_{01}$) until it reaches $\sigma_{ra}=p_a$ at A'. The radial stress at the expanding outer boundary $r=c$ of this zone remains at the yield point A. Continuity of radial stress and displacement across the internal boundary $r=c$ is imposed. The material in the outside zone, $c\leqslant r\leqslant b$ remains rigid, with the stress profile AB^0 as marked in Fig. 13, while the inner zone expands. The outer zone starts to yield when the circumferential stress component at $r=c$ (as AA' in Fig. 13) reaches the value of σ_{02} at a particular moment, which is when the outer zone ring reaches the thickness allowing to satisfy the yield condition, AB. The entire outer ring yields at the same instant and undergoes a *uniform* radial displacement $u=u_0$ as a consequence of the peculiar yield locus and the normality rule ($\dot{\varepsilon}_r=-\partial\dot{u}/\partial r=0$).

The moment of yielding onset of the outer ring is chosen as a starting point ($t=0$) for the subsequent phase, simulating a long-term process at a constant load driven by the chemical softening due to mass removal. The value of p_a determined by the deformed configuration at this particular moment is taken as the constant stress boundary condition that is applied to the grain during this phase of the process.

The numerical analysis of the boundary value problem focuses on the phase after the initial loading is completed and the radial stresses at the internal and external boundaries remain constant at $\sigma_{ra}=p_a$, $\sigma_{rb}=0$. At this point a phase of a time-dependent deformation begins driven by the chemical reaction of dissolution of silica. The material develops a simultaneous strain hardening and chemical softening via the compensatory mechanism mentioned already. Softening within the outer zone takes place due to dilatancy caused by yielding and producing new interface surface area for dissolution in addition to the original interfacial dissolution surface present within the material. The strain hardening generated via the compensatory mechanism drives the displacement at the inner boundary. With time progressing, the stress at boundary c grows along AA', while the boundary between the zones moves now inward, $\dot{c}<0$. The inner zone becomes smaller and the outer zone of dilatancy expands. That makes a total production of dissolved mineral larger and larger. With the choice of the simple yield function, the following constraints are imposed: for the inner zone, $a\leqslant r\leqslant c$, stress states stay at the corners (between A and C in Fig. 13) of

the subsequent yielding curves (see Fig. 13). The flow rule at the corner points is non-unique, but on the other hand, σ_r and σ_θ are in constant relation: $-\sigma_\theta/\sigma_r = \tan\varphi$. The latter condition, together with the strain hardening function, impose a contractile kinematics in the inner zone; for the outer zone, $c \leqslant r \leqslant b$, the yielding is determined by its circumferential stress component, hence $\dot{\varepsilon}_r = 0$, and $u = u_0 = \text{const}$. The normal (radial) stress component is required by equilibrium condition to be continuous across the boundary $r = c$, hence $\sigma_{rc}^{\text{inner}} = \sigma_{rc}^{\text{outer}}$. On the other hand, as the kinematics of the problem excludes the portions FD, EF and AD, the circumferential stress component becomes constrained by the requirement that stress at the interface $r = c$ remains at point A of the intersection of the yield condition and the critical state line, hence $\sigma_{\theta c}^{\text{inner}} = \sigma_{\theta c}^{\text{outer}}$. With these conditions and Eqs. (12)–(17), the internal pressure–displacement relationship can be determined as a solution of the following system of transcendental equations for the coupled chemo-mechanics in the outer zone, $c < r < b$:

The radial stress continuity requires that

$$\frac{p_a}{\sigma_{01}\tan\varphi}\left(\frac{a}{c}\right)^{1+\tan\varphi} = (1 - K_c t)\left(\frac{b}{c} - 1\right) - \left(\frac{\int_0^t K u_0\,\mathrm{d}t}{r} - \frac{\alpha u_0}{r}\right)\ln\frac{b}{c} \tag{18}$$

while the intersection of the yield locus and critical line requires the equality of circumferential stress components

$$\frac{p_a}{\sigma_{01}}\left(\frac{a}{c}\right)^{1+\tan\varphi} = (1 - K_c t) - \left(\frac{\int_0^t K u_0\,\mathrm{d}t}{r} - \frac{\alpha u_0}{r}\right) \tag{19}$$

Finally, the displacement at radius a, or indenter penetration is derived from the hardening function of the portion AB of the locus, as follows:

$$\frac{u}{r} - \frac{u_0}{c} = \frac{1}{\alpha}\left\{\frac{p_a/\sigma_{01}}{1+\tan\varphi}\left[\left(\frac{a}{r}\right)^{1+\tan\varphi} - \left(\frac{a}{c}\right)^{1+\tan\varphi}\right] + \ln\frac{r}{c}\right\} \tag{20}$$

where the chemical coefficients $K = \beta'\Xi k_+$ and $K_c = \beta'\Xi_0 k_+$ represent the chemical softening associated with dilatancy and the initial micro-cracking, respectively. The inner zone is contractile in the pre-creep phase, and it remains contractile across most of its thickness. The pre-existing void surface does generate some limited dissolution proportional to term Ξ_0 in Eq. (17), but its effect on chemical softening can be disregarded as physically immaterial. There is a narrow dilatant ring induced by the kinematic continuity condition across $r = c$, as seen in Fig. 14b. However, the dissolution from this zone is very limited and has been neglected in the simulation. The zone itself has a numerically insignificant thickness.

The results of the numerical solution of the equation system (18)–(20) are shown in Figs. 14–16. The values of the input parameters used are: $p_a/\sigma_{01} = 1.846$, $-\sigma_{02}/\sigma_{01} = \tan\varphi = 0.2$, $\alpha = 5$, $b/a = 10$. Fig. 14a represents the kinematics of the grain under the constant load, and shows the displacement u_a of the internal circumference, $r = a$, induced purely by the chemical process. This displacement can be interpreted as the penetration of the rigid asperity into the grain. As can be seen the chemical softening due to dissolution of the material can significantly accelerate the penetration, as coefficient K is proportional to both the rate dissolution constant and the chemical softening parameter. Fig. 14b illustrates the development of the different zones across the grain, at a given time, t. In particular, one may observe here the chemical coupling at the field level. In fact, for larger values of chemical coefficient K, the critical state zone ($r < c$) and compaction zone become smaller and disappear all together earlier, showing clearly that the dilatant damage zone is markedly increased due to the chemical reaction enhancement of damage (softening). The evolution of the distribution of the relative mass dissolution and volumetric strain is depicted in Fig. 15a and b, respectively. As the mass dissolution rate is proportional to dilatancy, the largest mass dissolution takes place close to the critical radius ($r = c$), usually the peak of negative volumetric strain.

As for the stress, being under a constant radial external loading, the radial stress distribution (Fig. 16a) does not

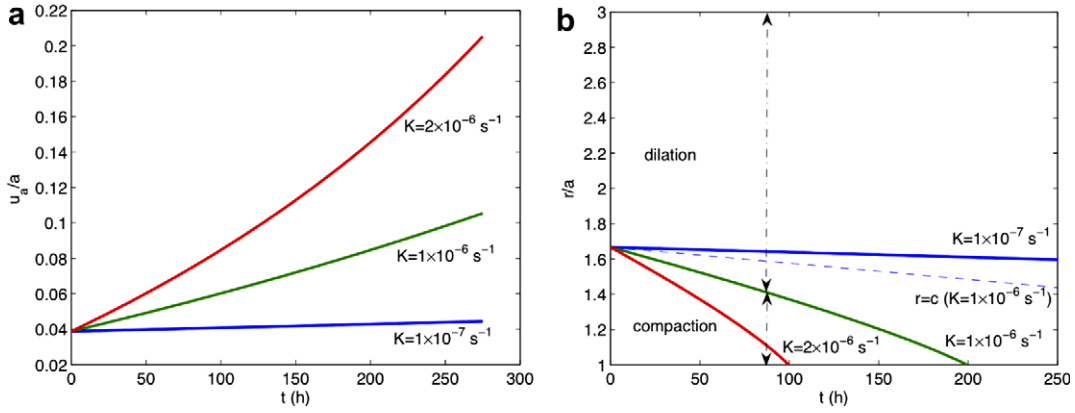

Fig. 14. (a) Penetration of intergranular contact; (b) propagation of zones.

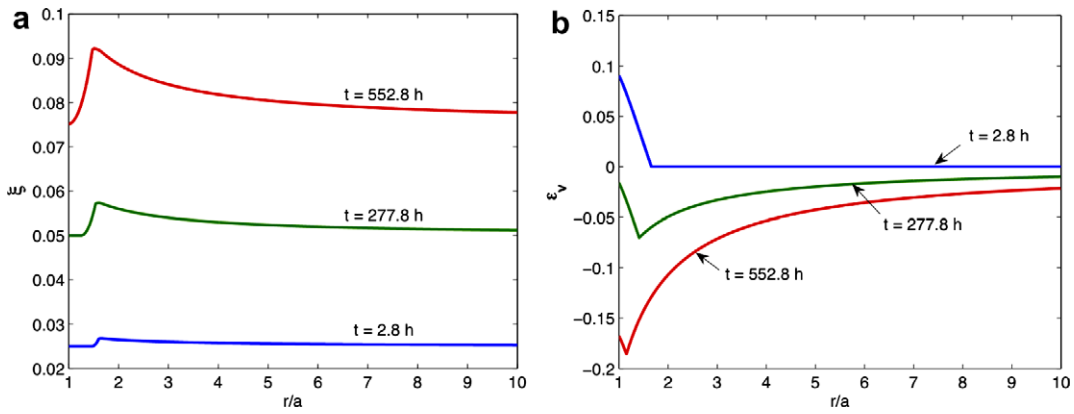

Fig. 15. (a) Evolution of the relative mass dissolution; (b) evolution of volumetric strain.

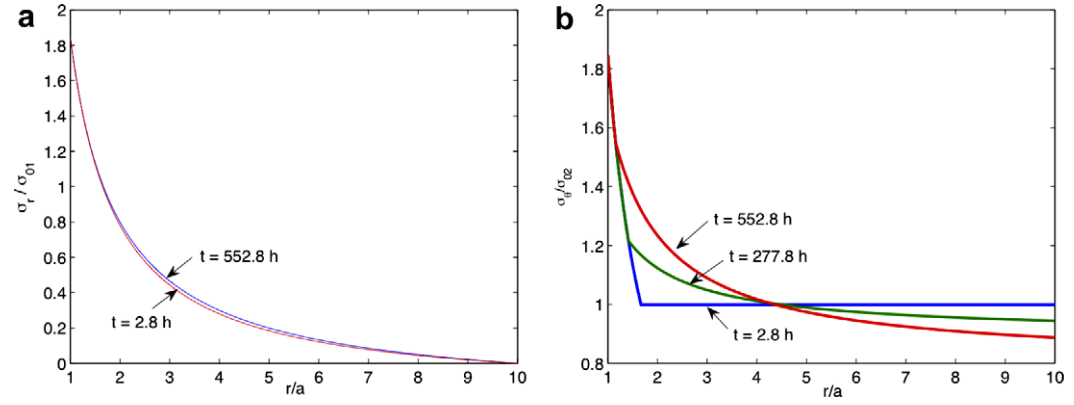

Fig. 16. (a) Evolution of the radial stress; (b) evolution of the circumferential stress.

change much. However, the circumferential stress distribution evolves quite significantly, as can be seen in Fig. 16b.

5.5. Intra-granular reactive transport at the micro-scale

In the following sections we investigate further various consequences of the grain contact processes, namely: transport of solutes across the intra-granular porous solid as well as transport within the intergranular pore, and finally precipitation over a medium range distance within the intergranular pore space.

First, an intra-grain diffusion of the dissolved matter away from the source at the newly created crack walls is addressed.

The intra-granular transport originates at the dissolution sites and, via the evolution of the dissolution surface area per unit volume, is coupled to the amount of deformation/damage. The presence of diffusion in turn affects the rate of mass change of silica, which is hence controlled by the reactive-diffusive transport law of silicic acid:

$$\frac{\partial x_{H_4SiO_4}}{\partial t} = D\left(\frac{\partial^2 x_{H_4SiO_4}}{\partial r^2} + \frac{1}{r}\frac{\partial x_{H_4SiO_4}}{\partial r}\right) + \frac{k_+(\Xi\varepsilon_v + \Xi_0)}{s} \qquad (21)$$

where $x_{H_4SiO_4}$ is molar fraction of aqueous silica in the fluid phase within the grain. Assuming the pore fluid, F to be a dilute solution, the molar fraction of any of its species k, has mass content $m_{kF} = M_{kF}/V_0$, linked to molar fraction, x_{kF} through V_0 which is the reference volume of the entire grain medium. D is the solute diffusion coefficient. The last term of the right-hand side in (21) is the rate of quartz mass production as defined in Eq. (5) via the activity of aqueous silica. Molar fraction is related to activity of an individual species determined by the constitutive law (1,2) and hence,

$$a_{kF} = \gamma_{kF} x_{kF}; \quad x_{kK} = \frac{N_{kK}}{\sum_{l\in K} N_{lK}} = \frac{m_{kK}/m_k^{(M)}}{\sum_{l\in K} m_{lK}/m_l^{(M)}} \qquad (22)$$

where N_{kL} is a number of moles of the species in the phase, $m_k^{(M)}$ is its molar mass.

Quartz mass production is enhanced by the dilatancy-damage of the grain material represented by the volumetric plastic strain. The dissolution rate is proportional to the reaction area $\widetilde{A}$, which is assumed to be a linear function of dilatant volumetric strain ε_v in Eq. (9). The local (micro-scale) precipitation is ignored. As $\varepsilon_v = -u_0/r$, the last term of Eq. (21) is determined independently from the solution of the system (18)–(20), which makes the transport

of aqueous silica deformation dependent on the deformation of the grain.

There are two stages of the intra-grain transport process as represented in the cartoon in Fig. 17. The reference conditions at a zero load are defined by a uniform dissolution of silica occurring within the body of the grain at the surface of pre-existing uniformly distributed voids, and directed toward the exterior of the grain. Interconnected intra-grain porosity, mainly at inter-crystalline boundaries, provides pathways for the transport. As only a subdomain of the entire grain is represented in our axisymmetric BVP, centered around the indenter, the reference stage is represented by a purely diffusive transport in a steady state. Concentration boundary conditions within the grain are: at the indenter, in contact with the macro-pore water continually washing the grain surface, a zero silicic acid concentration: $r = a,\ x_{H_4SiO_4} = 0$; the external boundary of the damaged zone within the grain at $r = b$ is an artificial boundary and in this BVP it represents the state in the undamaged part of the grain with dissolution from the pre-existing pores, in equilibrium with the solution in the macro-pore across its perimeter, and hence a constant concentration of silicic acid, $r = b,\ x_{H_4SiO_4} = x_0$ for $t \geqslant 0$. These boundary conditions imply also that there is an initial background steady-state transport following a classical diffusion solution, for a cylinder $b \geqslant r \geqslant a$, at $t = 0$, $x = \frac{\ln(r/a)}{\ln(b/a)} x_0$ (a standard solution that can be found in classical mass or heat transfer textbooks, see e.g. [59]), from the body of the grain to the point of contact with the indenter, or toward the macro-pore space, driven by the difference in the imposed values of concentration.

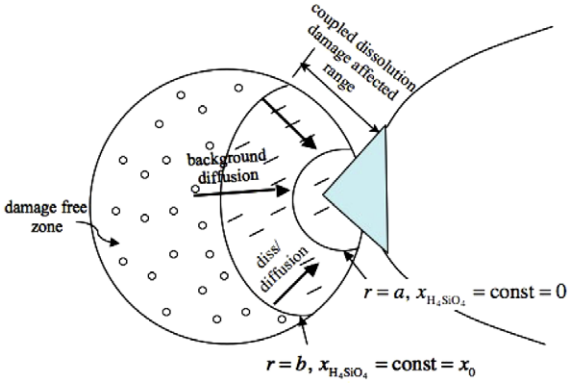

Fig. 17. Schematic representation of intra-grain transport.

Subsequently, a point-wise production of silicic acid across the damaged part of the body of the grain, coupled to the amount of mechanical damage evolves from the initial steady-state diffusion and affects the concentration distribution and consequently, the flux of the solute mass at the inner boundary. Such a diffusive flux, defined as $J = -D\nabla x_{H_4SiO_4}$ is of significant interest, as it allows one to determine the influence of the mechanical damage on the net dissolution of the grain and mass production of the solute. Fig. 18a and b show the flux of the material leaving the grain across the indent contact surface idealized as a cylinder at $r = a$. Non-dimensional variables of time and flux, respectively, τ and j are introduced as, $\tau = tD/a^2$ and $j = Ja/Dx_0$. Coefficient M represents the effect of deformation/damage associated with the dilatant volumetric strain on the mass transfer, $M = \Xi k_+ a^2/Dx_0$. The difference between the curves for $M = 5$ and $M = 0$ shows the disparity between chemo-mechanical and purely diffusive flux of the dissolved mineral. It is clear that the total flux is strongly dominated by the damage component.

6. Meso-scale model of grain assembly: transport phenomena and material stiffening

6.1. Inter-grain pore transport

We keep in mind one possible engineering application of the presented study, which is the prediction of compaction of soils and sediments at a constant in situ stress, prior, during and after the pore fluid (water, oil, natural gas) extraction. The above-mentioned aspects of the solute fate play a cardinal role in the extraction technologies and the consequent subsidence of soil/sediment masses.

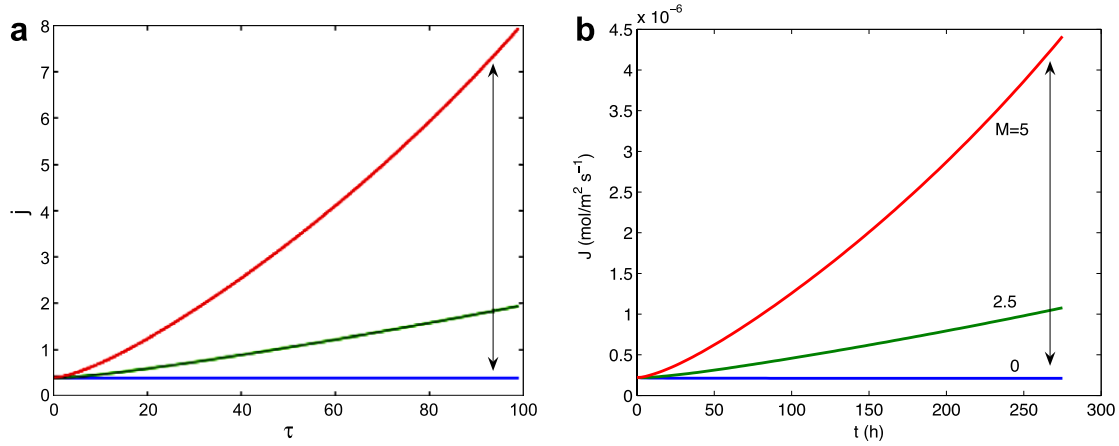

Fig. 18. (a) Evolution of the dimensionless flux at $r = a$; (b) evolution of the specific mass flux at $r = a$.

As mentioned earlier the fate of the dissolved mineral remains largely a mystery. Apparently contradictory laboratory and field evidence (see e.g. [13]) point to different scenarios. A standard scenario calls for a mid-range diffusive/advective transport of the dissolved species from the inter-grain boundary toward the macro-pore space and precipitation within it, at unstressed free surfaces (closed system scenario). An alternative scenario includes a transport (diffusive and/or advective) outside of the representative elementary volume and precipitation at a remote location (open system scenario). In this section we address a closed system scenario.

The mineral mass injected from the grain into the external pore water is assumed to be continuously washed away from the contact zone into the inter-grain pore space. Subsequent transport of the dissolved mineral in the inter-grain pore is assumed to be a mid-range transport, that is within one immediately adjacent inter-grain pore. It is conceptualized as a meso-scale reactive diffusion around individual grains filling the meso-scale pore. The mineral mass removed from the contact zone is transported and precipitated along the adjacent free surface of the grain. A "coating"-like precipitate accumulates on the free surface of the grain boundary reducing as a result the meso-pore space, as discussed in the next section.

In a particular configuration of the regular grain system (Fig. 19), a transport equation similar to Eq. (21) could be established, with the precipitation of aqueous silica considered instead of the dissolution term:

$$\frac{\partial x_{H_4SiO_4}}{\partial t} = \frac{D}{R^2}\frac{\partial^2 x_{H_4SiO_4}}{\partial \theta^2} - k_{-} x_{H_4SiO_4} \tag{23}$$

where D is the diffusion coefficient, k_{-} is the rate constant of precipitation. $x_{H_4SiO_4}$ is the molar fraction of aqueous silica in the inter-grain pore solution, $x_{H_4SiO_4} = x_{H_4SiO_4}(\theta, t)$, where θ represents the angular coordinate along the grain circumference surface, assumed as cylindrical, between A ($\theta = -\pi/4$) and B ($\theta = \pi/4$) as shown in Fig. 19. The first term on the right-hand side of Eq. (23) is the diffusion part of transport and the second term represents production part, in which only the precipitation is considered. In this equation it is assumed that transport takes place only at the free surface of the grain and the resulting precipitation accumulates forming a layer. This is indeed a highly idealized scenario, however, it provides a viable way to calculate the precipitated mass without considering the complicated path of the transport of the dissolved mass near the grain contact. Moreover, as pointed out in the later context, the mass conservation can directly give the precipitation rate quantity for a closed system without any geometrical considerations. The flux generated at the contact surface, f_p, discussed in the previous section determines the boundary flux condition for the above Eq. (23), considering a mass balance via

$$f_p = \frac{J_a \pi a}{4\varpi_p} \tag{24}$$

Eq. (24) is obtained by assuming that the amount of silicic acid (in terms of the number of moles) coming out from the contact area into the pore space is equal to the amount entering the transport path along the free surface of four one-quarter grains surrounding the contact. Thus, $J_a \cdot \pi a \cdot 1\ \mathrm{m} = 4 f_p \omega_p \cdot 1\ \mathrm{m}$. J_a is the mass flux produced by the grain across the inner boundary of the damage zone, $r = a$; ϖ_p is a hypothetical characteristic length of the pore space, which is postulated as the ratio of the volume of the macro-pore, V_{void} to the free surface area S_{free} of the grain exposed to the pore fluid, $\varpi_p = V_{void}/S_{free} = (2/\pi - 1/2)R$. The solution of Eq. (23) yields the precipitation flux and furthermore, the "coating" rate at the free grain surface, since the precipitated silica is assumed to form a coating-like layer.

Clearly, as the boundary flux f_p, Eq. (24), is time dependent, the transport process described by Eq. (23) is a transient process. A simplified solution is obtained by assuming that the chemo-mechanical coupling of the contact dissolution is a dominant process with respect to the transport and precipitation, and that Eq. (23) is addressed for a steady state, $\partial x_{H_4SiO_4}/\partial t = 0$. Hence, solving Eq. (23) with the boundary condition, $\theta = -\pi/4$: $D/R \cdot \partial x_{H_4SiO_4}/\partial\theta = f_p$ and $\theta = \pi/4$: $D/R \cdot \partial x_{H_4SiO_4}/\partial\theta = -f_p$ yields the concentration distribution as a function of θ:

$$x_{H_4SiO_4} = f_p \sqrt{\frac{1}{k_{-}D}} \frac{\exp\left[\sqrt{\frac{k_{-}R\theta}{D}}\right] + \exp\left[-\sqrt{\frac{k_{-}R\theta}{D}}\right]}{\exp\left[\sqrt{\frac{k_{-}}{D}}\frac{\pi R}{4}\right] - \exp\left[-\sqrt{\frac{k_{-}}{D}}\frac{\pi R}{4}\right]} \tag{25}$$

Notably, f_p as seen in Eq. (24), is a rate and hence bears dimension of t^{-1}. Consequently, the rate of the formation of coating can be calculated as a change in the coating thickness, over an infinitesimal area, $\mathrm{d}S$ of the free surface, as certain number of moles of silica are precipitated in the water volume, $\mathrm{d}V$,

$$\dot{d}_c = \frac{\mathrm{VOL}_{pre}}{\mathrm{d}S} = \frac{\mathrm{MOL}_{pre} v_{SiO_2}}{\mathrm{d}S} = \frac{k_{-} x_{H_4SiO_4} \cdot \mathrm{d}V \cdot v_{SiO_2}}{v_{H_2O}\mathrm{d}S} = \frac{k_{-} x_{H_4SiO_4} \varpi_p v_{SiO_2}}{v_{H_2O}} \tag{26}$$

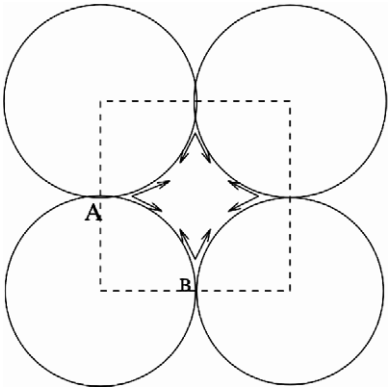

Fig. 19. A simple cell of grain system around the meso-pore.

Since practically $\sqrt{\frac{k_-}{D}}R \ll 1$, by considering a dilute solution, so that $e^x = 1 + x$ for $x \to 0$, Eq. (25) could be further linearized and the coating rate becomes

$$\dot{d}_c = \frac{J_a a \upsilon_{SiO_2}}{R \upsilon_{H_2O}} \tag{27}$$

where υ_{SiO_2} and υ_{HO_2} are the molar mass of SiO_2 and H_2O, respectively. As a result of this approximation, the coating rate appears to be uniformly distributed, i.e. independent of θ. The relative coating rate $(\dot{d}_c/R)$ is plotted against time as in Fig. 20a. It should be pointed out that this precipitation rate and the "coating" rate could be directly obtained by considering the mass conservation in a closed system (see e.g. [17]).

6.2. Meso-scale chemically driven pore volume reduction

From the engineering point of view one of the most important effects of intergranular contact phenomena is the macroscopically observed post-aging stiffening. The stiffness of a porous medium may be seen as primarily depending on the size of the pore. Hence, the stiffening may be seen as a product of a gradual filling of the pore with the load carrying precipitate. However, as the microscopic model presented in the previous subsection is limited to the phenomena within or around a single grain, it does not include the inter-grain pore. Inclusion of inter-grain pore requires considering an assembly of grain. A simple way to study the stiffening of a grain assembly is to consider a cluster of grains surrounding a pore. We will refer to such a system as the meso-scale model. Hence, to link the cause to the effect we need to cross the scale boundaries, to be able to use the variables pertinent to micro-scale at the meso-scale. Thus, up-scaling will be undertaken via averaging.

We consider a very simple geometric configuration of a 2D regular grain assembly as in Fig. 19, as a unit cell composed of four 1/4 grains, which henceforth becomes a representative volume at the meso-scale.

The initial macroscopic porosity of this volume is

$$\begin{aligned} n^0 &= \frac{V^0_{\text{void}}}{V^0} = 1 - \frac{V^0_{\text{solid}}}{V^0} \\ &= 1 - \frac{\pi R^2 - 8\left(\frac{R^2\theta_a}{2} - \frac{a_0\sqrt{R^2 - a_0^2}}{2}\right)}{4(R^2 - a_0^2)} \end{aligned} \tag{28}$$

where $\theta_a = \arcsin(a/R)$. V^0 is the initial volume of the unit cell and V^0_{void} is the initial volume of the void. a is the radius of the circular contact area between two grains. Initially, this contact radius is a_0. Numerically, it is equal to the inner radius of the damage zone of the grain, as in Section 5.4.

As discussed in the previous sections, the change of the macro-pore volume results from two geometrical changes: the approach of the grains caused by the grain deformation induced by a time-dependent chemo-mechanical indentation process at the intergranular contact, u_a, and the pore volume change due to mass precipitation on the pore walls. The deformation effect can be represented using an equation similar to (28) with the current contact radius approximated by $a = a_0 + u_a$:

$$\frac{V'_{\text{void}}}{V} = 1 - \frac{V'_{\text{solid}}}{V} = 1 - \frac{\pi R^2 - 8\left(\frac{R^2\theta_a}{2} - \frac{a\sqrt{R^2 - a^2}}{2}\right)}{4(R^2 - a^2)} \tag{29}$$

On the other hand, the relative pore space reduction in volume by the precipitation of the mineral at the free surface is controlled by the rate of coating

$$\frac{V''_{\text{solid}}}{V} = \frac{\int_0^t \dot{d}_c(2\pi - 8\theta_a)R\mathrm{d}t}{4(R^2 - a^2)} \tag{30}$$

Hence the total change of mesoscopic porosity could be defined as

$$-\Delta n = n_0 - n = \frac{V'_{\text{solid}}}{V} + \frac{V''_{\text{solid}}}{V} - \frac{V^0_{\text{solid}}}{V^0} \tag{31}$$

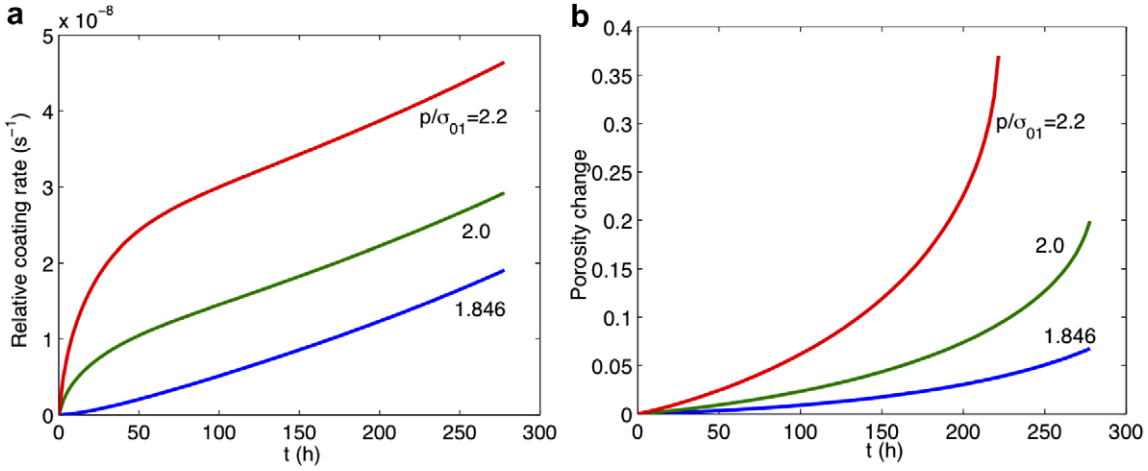

Fig. 20. (a) Evolution of relative coating rate; (b) evolution of porosity change, under different intergranular pressure.

The porosity evolution under different constant stress is presented in Fig. 20b.

6.3. Meso-scale representation of material stiffening due to precipitation

For the purpose of capturing the post-aging stiffening consider the meso-scale system of the four cylindrical particles in contact as in Fig. 19, but now under a uniform increment of load. These particles correspond to the mutually indenting cylindrical particles discussed in the previous section, which are additionally coated with a layer of the precipitate with a thickness corresponding to the length of time period of aging. As a unit cell we identify a set of four quarters of particles in contact. We put forward now a hypothesis that the deformability of such a system is controlled by the relative size of the meso-pore. We then represent the neighborhood of the meso-pore as a hollow cylinder subject to a compressive external loading. Its configuration and boundary conditions are presented in Fig. 21. Consequently, the system presented is meant to simulate the variable compressibility of the porous medium dominated by the "arching" action around the pore of radius r_i decreasing in time due to mineral precipitation.

The compressibility of the system can be quantified by a relationship between the external displacement u_e at the external radius $r = r_e$, or a direct result of average volumetric strain based on the displacement calculation, and the pressure p at $r = r_e$. The stiffness evolution is followed by parameterizing the stiffness with respect to a decreasing of the internal radius. The entire process of aging is simulated by a compression loading in three phases. Here, the same rigid-plastic constitutive relationship (Fig. 13) used in early discussion on a micro-scale granular contact, is adopted, but to represent the yield condition of such a REV in a different scale. The solution procedure for pre-aging phase and aging phases follows the same spirit as in Section 5.4 and is briefly summarized below.

Pre-aging (OA in Fig. 22) is the phase in which the external load σ_{re} is increased from 0 to p_e^c. The solution is obtained in a similar way as for the intergranular contact model (Section 5.4). The yield function and kinematic condition determine the stress profile as shown in Fig. 13. The stress state at the inner boundary $r = r_i$ is initially represented by point J, then moving along the σ_θ axis. The problem is solved with a similar approach, in which, however, only one-zone configuration is considered. This configuration is ensured for the cylinders for which $r_e/r_i < 2.718$, that is for the media with the porosity larger than 13.5%. Under these restrictions, the entire cylinder is subjected to the yield condition depending on the circumferential stress and because of the associated kinematics ($\dot{\varepsilon}_r = \partial\dot{u}/\partial r = 0$) undergoes a uniform radial displacement rate. Consequently, as shown in Fig. 22, the slope of the pressure–displacement curve is $\alpha \ln(r_e/r_i)$.

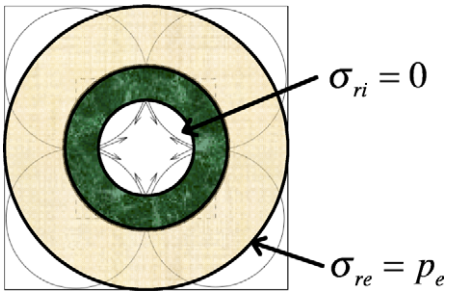

Fig. 21. Representation of a meso-scale REV subjected to the post-aging load increment.

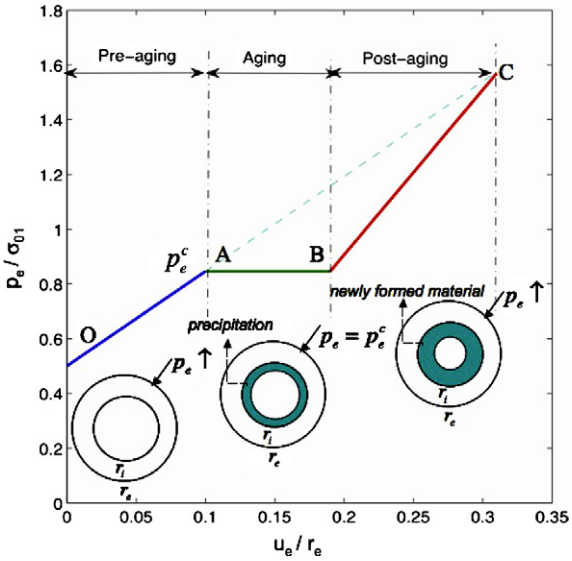

Fig. 22. Pressure–displacement curve for different phases during compression of a meso-scale REV.

Aging (AB in Fig. 22) corresponds to the phase of a constant external load $\sigma_{re} = p_e^c$. Due to the chemical softening effect, the strain is developing. However, as the mechanism of chemical softening and plastic strain is localized within a narrow zone of a single grain, we shall directly adopt upscaled values of mass dissolution from the micro-scale mechanism discussed in Section 5.4, as calculated over the four grains. Consequently, the yield criterion and equilibrium provide the corresponding stresses. Note, that it is assumed that the behavior of the meso-scale grain system as represented in Fig. 21 is not sensitive *during* aging to the effect of precipitating mineral. This is an approximation supported by the observation that precipitation occurs at a high circumferential stress and hence at a predeformed surface of the grain. Therefore, the coating layer at the moment of deposition has a zero strain. It may be expected that in reality some further aging strain induces an incremental strain in the coating layer, and hence some stress, but it is believed that this effect is minor.

The post-aging phase starts when after a period of aging, the load at $r = r_e$ resumes to increase above the value of p_e^c. A peculiarity of this phase is the presence of the newly formed material, which has precipitated on the surface of the pore, i.e. at $r < r_i$. It is hypothesized that material has the same mechanical constitutive properties

as the original material (this assumption is not necessary but yields a very simple mathematical solution). Hence the response to the further compression is strongly dependent on the size of the inner radius. The pressure–displacement response becomes stiffer as the post-coating inner radius is smaller due to the precipitated mass. Similar to the pre-aging phase, the slope of the post-aging compression line (BC in Fig. 22) is determined as $\alpha \ln(r_e/(r_i - \Delta_i))$. Δ_i is the thickness of the coating layer. In this particular presentation for the purpose of demonstrating the stiffening effect, we consider a uniform Δ_i calculated directly from the relative mass dissolution:

$$\Delta_i = \frac{\zeta_p V_S}{A_{free}} = \frac{v_p \zeta_d V(1-n)}{A_{free}} \tag{32}$$

In general, ζ_p is the relative mass precipitation, obtained by averaging the coating rate $\dot{d}_c$ over time and free surface within a meso-REV, $\zeta_p = \int_t \int_{A_{free}} \dot{d}_c \, dA_{free} \, dt/V_S$. We define ζ_d as the accumulated relative mass dissolution at the meso-scale, calculated with a cross-scale function $\zeta_d = \int_t \int_{V_S} \dot{\xi} \, dV \, dt/V_S$ by integration of $\dot{\xi}$ over time and the entire volume of the solid grains in a meso-scale REV. For the purpose of addressing the stiffness change via a solution to the meso-scale BVP. A coating is represented as a corresponding change in internal radius directly from the precipitated mass via Eq. (32). V consists of the total volume of the grains as well as the pores in the meso-scale REV, hence, $V = \sum_k V_{Gk} + V_P$, V_{Gk} is the volume of an individual grain and V_P is the volume of the pores in a meso-scale REV. v_p represents the ratio of precipitated mass to the total accumulated relative mass dissolution as not all the mass dissolved must precipitate locally (for a an open system, with a vigorous stirring effect it may happen that $v_p = 0$), n is the porosity and A_{free} is the free surface area in the total volume V, of a meso-scale REV.

It needs to be noted that for the very simple form of the yield surface as presented in Fig. 13, the compression of the hollow cylinder is always stable. This would not be the case for a more realistic form of the yield criterion allowing for a mechanical strain softening. For such a case Hueckel and Mróz [57] have shown that after an initial phase of an increased pressure, a hollow cylinder undergoes an unstable phase when at a continuing closure of the pore the external pressure actually decreases. This type of behavior matches the macroscopically observed end of precipitation enhanced post-aging stiffening effect. Further possible refinements of the problem formulation should first of all include a different strength and hardening characteristics of the precipitate material, as compared to the original material.

7. A macro-scale constitutive law: effects of the micro-scale mass removal and precipitation. Cross-scale transfer functions

We will employ previously proposed macroscopic chemo-plasticity theory [1,2], which is an extension of Cam-clay theory of hardening plasticity [60]. Its main tool is the yield limit usually expressed in terms of mean normal stress $\bar{p}$ and deviatoric stress invariant $\bar{q}$ expressed as $\bar{q} = \left(\frac{1}{2}\bar{s}_{ij}\bar{s}_{ij}\right)^{1/2}$. Variables marked with a top bar refer to macro-scale, if they were previously used at micro- or meso-scale

$$f = \bar{p}^2 - \bar{p}p_c + (\bar{q}/M)^2 = 0 \tag{33}$$

The hardening variable p_c, describing the size of the yield locus and hence the apparent preconsolidation stress, is proposed to be dependent, classically, on the volumetric plastic strain and the relative mass change due to dissolution and precipitation. As clearly learned from the previous sections, the net change of mass of mineral per unit volume of the macrostructure has no specific meaning, as the removed or added masses play a fundamentally different structural role in the granular assembly. Also importantly, these masses are removed from or added to "strategically" different locations in the macrostructure. In other terms, even though the removed and added masses are of the same mineral and within the same macro-REV, their structural role is different, and they need to be treated differently in the macroscopic constitutive law (33). The only way we were able to envision to accomplish this task is to relate the masses of the same species to lower scale variables explicitly and associate them with their corresponding different microscopic mechanisms. In what follows similar to Hueckel et al. [61], we associate the dissolved mass with a macroscopic chemical softening mechanism, whereas the precipitated mass with a macroscopic post-aging stiffening mechanism. As a result the hardening function p_c is postulated as

$$p_c = p_c^0 \exp\left\{[\lambda(\bar{\zeta}_p)]^{-1}(1+e_0)\bar{\varepsilon}_v^{pl} + R(\bar{\zeta}_d)\right\} \tag{34}$$

where p_c^0 is the initial size of the yield locus. e_0 is the initial void ratio. λ is the plastic (variable) bulk modulus of compressibility (logarithmic). To be consistent with the microscopic approach, rigid-plasticity is adopted. The chemical softening term R is a function of the macroscopic relative mass loss $\bar{\zeta}_d$. This mass loss can be identified as the volume average of a meso-scale mass removed from the solid grain, ζ_d integrated over the macro-REV. The expression for this volume average is effectively a cross-scale transfer function for the mass removal effect. In a normal compression test, λ describes the slope of change of the specific volume against change of the isotropic stress. A visible decrease in its value in the macro-scale post-aging phase experiments presented in Section 2 is of particular interest. We propose that λ depend on the amount of the mineral precipitated in the macro-pore during the aging phase, defined via a macroscopic variable $\bar{\zeta}_p$. In what follows it will be obtained as the volume average of the relative mass over the meso-REV. The expression for this volume average is a cross-scale transfer function for the added mass effect. This separation of roles could be proved directly by performing closed system and open system experiments, removing in the latter one, all dissolved mass from the suspension by flushing the pore space with a fresh pore fluid.

Hence, compressibility modulus λ is expressed by

$$\lambda = \lambda_0 \Psi(\bar{\zeta}_p) \tag{35}$$

λ_0 is a constant (initial value of) stiffness modulus before aging. It may easily be obtained from a standard mechanical test.

The macroscopic tests make it possible to observe and measure a post-aging stiffness increase when the loading is resumed at the end of the aging. As the amount and the range of the stiffening increase with the amount of strain accumulated during aging (see Fig. 24) this can possibly be attributed to the contribution of the precipitated material to undertake additional loading after the loading resumes. It is however not known whether *during* aging itself the precipitated material actually contributes to carrying any load. Also, as can be seen at the meso-scale there is an upper limit of how much of the material can precipitate within a pore and hence there is a limit of the stiffness growth. Given these uncertainties it is assumed that the evolution of the yield limit during aging is affected by these two counteracting phenomena of macroscopically measured dissolution induced softening and precipitation induced hardening. However, it needs to be noted that the amount of the actually precipitated mineral depends also on factors like a long-range transport, such as diffusion and/or advection of the dissolved mineral outside of the macro-RVE. Therefore, two independent chemical variables need to be considered separately, and their effects on the preconsolidation need to be easily identifiable.

For a constant stress $\dot{\bar{\sigma}}_{ij} = 0$, or plastic-neutral loading $\frac{\partial f}{\partial \bar{\sigma}_{ij}} \dot{\bar{\sigma}}_{ij} = 0$ the resulting macroscopic plastic strain rate occurring during this aging process is obtained from the extended Prager consistency condition [46]

$$\dot{\bar{\varepsilon}}_v^{pl} = -\left(\frac{\frac{\partial f}{\partial \bar{\zeta}_p} \dot{\bar{\zeta}}_p + \frac{\partial f}{\partial \bar{\zeta}_d} \dot{\bar{\zeta}}_d}{\frac{\partial f}{\partial \bar{\varepsilon}_v^{pl}}} \right) \tag{36}$$

The macroscopic volumetric strain arises resulting from the compensation mechanism for the net resultant of the chemical softening and chemical hardening (stiffening). The identification of the variables used in the above macroscopic description of the plastic strain is much dependent on a good understanding of the chemo-mechanical coupling process at the micro-scale, as well as its subsequent consequence at the meso-scale discussed above. To be able to quantify the processes controlling dissolution softening and precipitation hardening one need to resort to numerical models at micro- and meso-scales. The formulation such as in Eqs. (33)–(36) requires a tool for linking these scale processes to macroscopic properties.

In what follows, we will use the results of microscopic and mesoscopic simulations developed in Sections 5 and 6 to determine the remaining macroscopic constitutive functions. Notably, the simulation of the post-aging stiffening can provide data for coefficient λ. From Eq. (35) one can determine that at the macro-scale the strain increments produced over an equal stress increment during pre-aging and post-aging phases are proportional to their respective moduli, λ_0 and λ

$$\frac{\lambda}{\lambda_0} = \frac{(\mathrm{d}\bar{\varepsilon}_v^{pl})^{post\text{-}a}}{(\mathrm{d}\bar{\varepsilon}_v^{pl})^{pre\text{-}a}} \tag{37}$$

Their values can be determined by considering the macroscopic volumetric strains as up-scaled mesoscopic variables of volume changes calculated as above (Fig. 22).

The above averaging procedures allow us to obtain, the hardening function Ψ and hence λ as functions of time, in terms of the chemical reaction rates and microscopic constitutive parameters. A special case examined here is taking the representing variables for a meso-REV in Fig. 21 as those for a macro-scale REV, assuming periodic arrangement of grain system and demonstrating a possible expression for the hardening function Ψ. We replace the radii, r_i and r_e with their expressions in terms of the macro-scale properties V, A_{free} and void ratio e, then utilizing Eqs. (32, 35, 37), the hardening function Ψ can be obtained as

$$\begin{aligned} \Psi = \frac{\lambda}{\lambda_0} &= \frac{(d\bar{\varepsilon}_v^{pl})^{post\text{-}a}}{(d\bar{\varepsilon}_v^{pl})^{pre\text{-}a}} \\ &= \frac{\Delta p \Big/ \left[\frac{\alpha(r_e + r_i - \Delta_i)}{2r_e} \ln(r_e/(r_i - \Delta_i)) \right]}{\Delta p \Big/ \left[\frac{\alpha(r_e + r_i)}{2r_e} \ln(r_e/r_i) \right]} \\ &= \left[1 - \frac{\bar{\zeta}_p}{2e + e\sqrt{1+e}} \right] \left[\frac{\ln \sqrt{1+e^{-1}}}{\ln \frac{2\sqrt{e(1+e)}}{2e - \bar{\zeta}_p}} \right] \end{aligned} \tag{38}$$

In turn, knowing the evolution of λ, the chemical softening term $R(\bar{\zeta}_d)$ in Eq. (35) can now be calculated using the data from the simulation of the micro-scale process of dissolution during aging and assuming it to be a linear function of the macroscopic relative mass dissolution $\bar{\zeta}_d$, i.e. $R(\bar{\zeta}_d) = R_c \bar{\zeta}_d$. Hence, returning to Eq. (36), the macroscopic variables $\dot{\bar{\zeta}}_d, \dot{\bar{\zeta}}_p$ and $\dot{\bar{\varepsilon}}_v^{pl}$ can be substituted by their counterpart averages at the meso-scale

$$R_c = -\left(\frac{\frac{\partial f}{\partial \bar{\varepsilon}_v^{pl}} \dot{\bar{\varepsilon}}_v^{pl} + \frac{\partial f}{\partial \bar{\zeta}_p} \dot{\bar{\zeta}}_p}{\dot{\bar{\zeta}}_d} \right) \tag{39}$$

Hence, knowing $\frac{\partial f}{\partial \bar{\zeta}_p}$, $\frac{\partial f}{\partial \bar{\varepsilon}_v^{pl}}$ and the averaged rates $\dot{\bar{\zeta}}_d, \dot{\bar{\zeta}}_p$ and $\dot{\bar{\varepsilon}}_v^{pl}$, coefficient R_c can easily be determined. In particular, the macroscopic strain could be described by the boundary displacement of the meso-scale REV:

$$\dot{\bar{\varepsilon}}_v^{pl} = \frac{\int_S u_i n_i \, \mathrm{d}S}{V} \tag{40}$$

V is the volume of the REV with the boundary surface S. u_i is the boundary displacement and n_i is the outer unit normal vector of S. It could be further simplified in a discrete form [62,58]:

$$\dot{\bar{\varepsilon}}_v^{pl} = \frac{\sum_L \Omega_i^c \Delta \dot{u}_i^c}{V} \tag{41}$$

$\Delta\dot{u}_i^c$ is the relative translation rate of the two grain centers of the edge c. Ω_i^c is the complementary area vector, a micro-variable that characterizes the local geometry of the neighborhood of cth edge. The above result is coincident with the result in Eq. (36) when the higher order of deformation gradient is ignored when only small strain is considered.

It should be pointed out that the porosity change due to precipitation reads

$$\dot{\bar{n}}^{\text{prec}} = \frac{\int_{A_{\text{free}}} \dot{d}_c \, \mathrm{d}A_{\text{free}}}{V} = \dot{\bar{\zeta}}_{\text{p}} \vartheta_S$$

ϑ_S is the volume fraction of solid grains in a macro-REV. Clearly, this effect is reflected by Eq. (36), in which the stiffness modulus is dependent upon the relative mass precipitation.

The above procedures make it possible to up-scale the meso-scale volumetric variables and pressures to the corresponding macro-scale quantities and identify the macro-scale constitutive parameters. Hence, the constitutive parameter of the macro-scale is

$$R_c = \frac{1+e}{\lambda}\left(\frac{\frac{1}{\lambda}\frac{\partial\lambda}{\partial\bar{\zeta}_{\text{p}}}\dot{\bar{\zeta}}_{\text{p}} - \dot{\bar{\varepsilon}}_{\text{v}}^{\text{pl}}}{\dot{\bar{\zeta}}_{\text{d}}}\right) \tag{42}$$

where $\partial\lambda/\partial\bar{\zeta}_{\text{p}}$ could be obtained from Eq. (38).

R_c could be approximately calculated using the upscaled values from the meso-scale model for a simple configuration as in Fig. 18. If the void ratio in Eq. (42) is chosen as the initial void ratio $e_0 = 0.258$, the initial stiffness modulus $\lambda_0 = 0.73$, the increment of plastic volumetric strain could be obtained from the formulae (28) and (31) (see also Fig. 20b) for the first 150 h, $\Delta\bar{\varepsilon}_{\text{v}}^{\text{pl}} = 0.024$. The relative mass dissolution is obtained by integrating over the four grains and the result is presented in Fig. 23. For simplicity it is assumed that the precipitated mass is equal to the dissolved mass. For such a period as 150 h, $\Delta\bar{\zeta}_{\text{d}} = \Delta\bar{\zeta}_{\text{p}} = 0.056$. The modulus λ can be calculated from Eq. (38), obtaining $\lambda = 0.59$, a nearly 20% decrease in the compressibility compared to the initial one in 6 days. Finally, the value of R_c is found from Eq. (42) as $R_c = -9.617$.

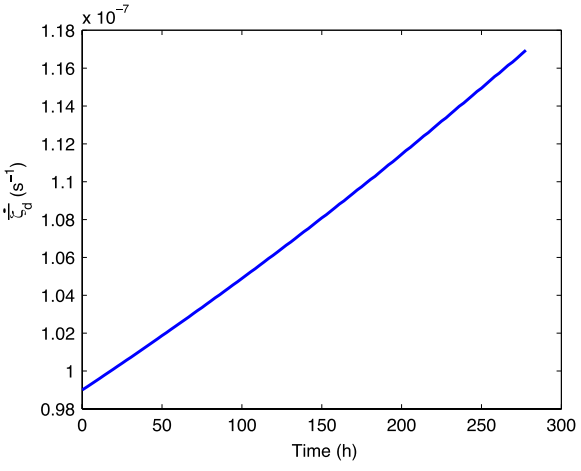

Fig. 23. Rate of the relative mass dissolution as upscaled from a meso-scale model.

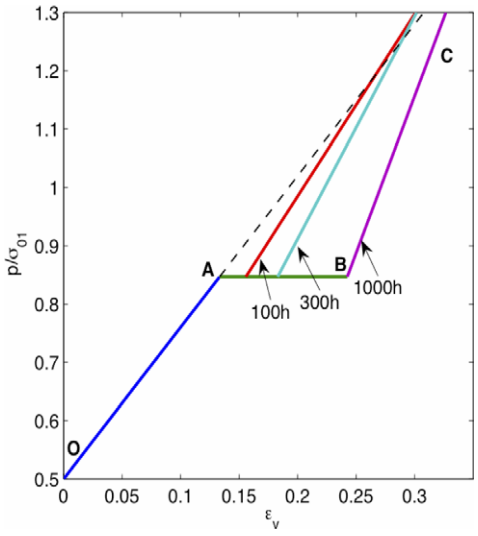

Fig. 24. Pressure vs. volumetric strain at macro-scale as upscaled from a meso-scale model.

As a result we can reconstruct a macroscopic representation of the post-aging stiffness. Clearly, as the thickness of the precipitation coating depends on the aging time period, so does the change in the post-aging compressibility. Fig. 24 represents such variation for a selected aging period duration values. Within 1000 h of aging an about 50% increase of the stiffness is reached. The general trend and numerical values compare satisfactorily with the experimental data in Fig. 1.

8. Conclusions

In this paper, dissolution of minerals at a stressed intergranular contact and its consequence are investigated via scenarios of chemo-mechanical processes hypothesized to develop during soil or sediment compaction. Some qualitative experiments on submerged solid grains of chalk in contact illustrate a damage-enhanced dissolution. These experiments together with geological evidence in the literature provide a motivation for the main hypothesis that the chemo-mechanical damage in the contact zone is largely responsible for the evolution of the sediment properties during compaction. A scenario has been constructed which includes: a chemo-mechanical model of indentation into rigid-chemo-plastic grain, producing significant enhancement of mineral dissolution and simultaneous chemical softening of the grains, followed by diffusion and precipitation at the free surfaces of the grain assembly. As a result of grain deformation and precipitation, a porosity evolution takes place.

A mathematical model developed to numerically describe this scenario is effectively a three-scale model. The scales are: micro-scale for intra-grain processes, meso-scale for processes within grain assembly and

macro-scale of a granular continuum. At each scale different BVPs are constructed to simulate numerically transport and deformation. At the stressed intergranular contact, a coupled model of chemical dissolution and damage of irreversibly deformed grain has been proposed. Chemical softening has been introduced via a novel softening variable of the specific free surface area. The indentation grows substantially with time as chemical weakening due to solid–fluid dissolution reaction becomes significant. This model makes possible to predict the porosity evolution of a very simple grain assembly under different pressures at the meso-scale and the evolution of the stiffness as a function of the aging duration and the associated stress at the macro-scale. A cross-scale transfer function (micro–meso and meso–macro) is necessary to differentiate the fate of the same mineral masses engaged in different processes within the same macroscopic REV.

The model has a value of a prototype. To make the calculations possible with the use of *Matlab*, elastic effects were neglected, the geometry of the contact is highly approximated using a well-known Johnson's hypothesis. Linearized yield locus, linear strain hardening functions as well as a linear reactive-diffusion transport model were employed. Hence, the results are qualitative rather than quantitative, but reproduce well the main phenomena and tendencies. They demonstrate the potential of such models in practical applications.

An important lesson from this exercise is that to formulate a model in terms of macroscopic variables, information is needed in terms of micro- or meso-scale variables quantifying the phenomena occurring at these scales, but affecting the macroscopic properties and behavior. This information is provided by the appropriately formulated cross-scale functions.

Acknowledgement

This work was partially supported by US National Science Foundation grant #0324543, Geomechanics and Geotechnical Systems Program.

References

[1] Hueckel TA. Water–mineral interaction in hydro-mechanics of clays exposed to environmental loads: a mixture theory approach. Can Geotechn J 1992;29:1071–86.
[2] Hueckel T. Reactive plasticity for clays during dehydration and rehydration. Part I: concepts and options. Int J Plast 2002;18(3):281–312.
[3] Hueckel T, Hu LB. Chemo-mechanical coupling and damage enhance enhanced dissolution at intergranular contact. In: Pande GN, Pietruszczak S, editors. Proceedings of the ninth symposium on numerical models in geomechanics, Ottawa, Canada, 2004. p. 349–53.
[4] Hueckel T, Cassiani G, Fan T, Pellegrino A, Fioravante V. Aging of oil/gas-bearing sediments, their compressibility, and subsidence. J Geotechn Geoenviron Eng, ASCE 2001;127(11):926–38.
[5] Schmertmann JH. The mechanical aging of soils. J Geotechn Eng, ASCE 1991;117(9):1288–330.
[6] Lessard G, Mitchell JK. The causes and effects of aging in quick clays. Can Geotechn J 1985;22(3):335–46.
[7] Bjerrum L. Problems of soil mechanics and construction on soft clays. In: Proceedings of the eighth international congress of soil mechanics and foundation engineering, 3, 1973. p. 111–59.
[8] Cassiani G, Zoccatelli C. Toward a reconciliation between laboratory and in situ measurements of soil and rock compressibility. In: Carbognin L, Gambolati G, Johnson AI, editors. Proceedings of the sixth international symposium on land subsidence, vol. 2, Padova. La Garsignola, 2000. p. 3–15.
[9] Hueckel T, Cassiani G, Prevost JH, Walters DA. Field derived compressibility of deep sediments of the Northern Adriatic. In: Barends FBJ, Carbognin L, Gambolati G, Steedman RS, editors. Land subsidence. Special volume: Multi-disciplinary assessment of subsidence in the Ravenna area. Rotterdam: Millpress; 2005. p. 35–51.
[10] Yamamuro JA, Lade PV. Experiments and modelling of silty sands susceptible to static liquefaction. Mech Cohes-Frict Mater 1999;4(6):545–64.
[11] Mitchell JK, Solymar ZV. Time-dependent strength gain in freshly deposited or densified sand. J Geotechn Eng, ASCE 1984;110(11):1559–76.
[12] Denisov NY, Reltov BF. The influence of certain process on the strength of soil. In: Proceedings of the fifth international conference, SMFE, 1(12), 1961. p. 75–8.
[13] Baxter CDP, Mitchell JK. Experimental study on the aging of sands. J Geotechn Geoenviron Eng, ASCE 2004;130(10):1051–62.
[14] Weyl PK. Pressure solution and the force of crystallization – a phenomenological theory. J Geophys Res 1959;64:2001–25.
[15] Rutter EH. The kinetics of rock deformation by pressure solution. Philos Trans R Soc A 1976;283:203–19.
[16] Lehner FK. A model for intergranular pressure solution in open systems. Tectonophysics 1995;245:153–70.
[17] He W, Hajash A, Sparks D. A model for porosity evolution during creep compaction of sandstones. Earth Planetary Sci Lett 2002;197:237–44.
[18] Ghoussoub J, Leroy YM. Solid-fluid phase transformation within grain boundaries during compaction by pressure solution. J Mech Phys Solids 2001;49(10):2385–430.
[19] Elliott D. Diffusion flow laws in metamorphic rocks. Geol Soc Am Bull 1973;84:2645–64.
[20] Tada R, Siever R. Pressure solution during diagenesis: a review. Ann Rev Earth Planet Sci 1987;17:89–118.
[21] Gratier JP. Le fluage des roches par dissolution–crystallisation sous contrainte dans la croûte supérieure. Bull Soc géol France 1993;164:267–87.
[22] Raj R, Chyung CK. Solution-precipitation creep in glass ceramics. Acta Metall 1981;29:159–66.
[23] Spiers CJ, Schutjens PMTM. Densification of crystalline aggregates by fluid phase diffusional creep. In: Meridith PG, Barber D, editors. Deformation processes in minerals, ceramics and rock. London: Unwin Hyman; 1990. p. 334–53.
[24] Durney DW. Solution-transfer, an important geological deformation mechanism. Nature 1972;235:315–7.
[25] Paterson MS. Nonhydrostatic thermodynamics and its geologic applications. Rev Geophys 1973;11:355–89.
[26] Dewers T, Ortoleva P. A coupled reaction-transport mechanical model for intergranular pressure solution stylolites, and differential compaction and cementation in clean sandstones. Geochim Cosmochim Acta 1990;54:1609–25.
[27] Subramonian SJ, Sofronis P. Modeling the interaction between densification mechanisms in powder compaction. Int J Solids Struct 2001;38:7899–918.
[28] Bathurst GC. Diagenetic fabrics in some British Dinantian limestones. Liverpool Manchester Geol J 1958;2:11–36.
[29] Rice JR, Chuang TJ. Energy variations in diffusive cavity growth. J Am Ceram Soc 1981;64(1):46–53.
[30] Cocks ACF. The structure of constitutive laws for the sintering of fine grained materials. Acta Metal Mater 1994;42(7):2191–210.
[31] Tada R, Siever R. Experimental knife-edge pressure solution of halite. Geochim Cosmochim Acta 1986;50:29–36.

[32] Tada R, Maliva R, Siever R. A new mechanism for pressure solution in porous quartzose sandstone. Geochim Cosmochim Acta 1987;51:2295–301.
[33] Ostapenko GT. Recrystallization of minerals under stress. Geochem Int 1968;5:183–6.
[34] Ostapenko GT. Theories of local and absolute chemical potential, their experimental testing and application of the phase rule to the systems with nonhydrostatically stressed solid phases. Geochem Int 1975;11:355–89.
[35] Bosworth RGC. Strain-induced preferential dissolution of halite. Amsterdam: Elsevier; 1981.
[36] Pharr GM, Ashby MF. On creep enhanced by a liquid phase. Acta Metall 1983;31:129–38.
[37] Milliken KL. The widespread occurrence of healed microfractures in siliciclastic rocks: evidence from scanned cathodoluminescence imaging. In: Nelson PP, Laubach SE, editors. Proceedings of North American rock mechanics symposium. Rotterdam: Balkema; 1994. p. 825–32.
[38] Dewers T, Hajash A. Rate laws for water-assisted compaction and stress-induced water–rock interaction in sandstone. J Geophys Res 1995;100:13093–112.
[39] Gratz AJ. Solution-transfer compaction of quartzites: progress toward a rate law. Geology 1991;19:901–4.
[40] den Brok SWJ. Effect of microcracking on pressure solution strain rate: the Gratz grain-boundary model. Geology 1998;26(10):915–8.
[41] den Brok SWJ, Spiers CJ. Experimental evidence for water weakening of quartzite by microcracking and solution-precipitation creep. Geol Soc (London) J 1991;148:541–8.
[42] Hickman SH, Evans B. Kinetics of pressure solution at halite–silica interfaces and intergranular clay films. J Geophys Res 1995;100(13):113–32.
[43] Zou M, Yang D. Nanoindentation of silica nanoparticles attached to a silicon substrate. Tribol Lett 2006;22(2):189–96.
[44] Hu LB. Chemo-mechanical coupling at the intergranular contact: a microscopic prototype model, MS Thesis, Durham, Duke University, North Carolina, 2004.
[45] He W, Hajash A, Sparks D. Creep compaction of quartz aggregates: effects of pore-fluid flow-a combined experimental and theoretical study. Am J Sci 2003;303:73–93.
[46] Hu LB, Hueckel T. Creep of saturated materials as a chemically enhanced rate dependent damage process. Int J Numer Anal Methods Geomech, in press. doi:10.1002/nag.600.
[47] Hueckel T, Pellegrini R, Del Olmo C. Constitutive properties of thermo-elasto-plastic behavior of deep carbonatic clays. Int J Numer Anal Methods Geomech 1998;22(7):549–76.
[48] Rimistid JD, Barnes DL. The kinetics of silica–water reaction. Geochim Cosmochim Acta 1980;44:1683–99.
[49] De Groot SR. Thermodynamics of irreversible processes. Amsterdam: North Holland; 1966.
[50] Brace WF, Paulding BW, Scholz CH. Dilatancy in the fracture of crystalline rocks. J Geophys Res 1966;71:3939–53.
[51] Scholz C. Micro fracturing and the inelastic deformation of rock in compression. J Geophys Res 1968;73:1447–54.
[52] Hueckel T, Borsetto M. Thermoplasticity of saturated soils and shales: constitutive equations. J Geotechn Eng, ASCE 1990;116(12): 1765–77.
[53] Johnson KL. The correlation of indentation experiments. J Mech Phys Solids 1970;18:115–26.
[54] Johnson KL. Contact mechanics. Cambridge: Cambridge University Press; 1985.
[55] Hill R. The mathematical theory of plasticity. Clarendon Press; 1950.
[56] Mróz Z, Kwaszczynska K. Certain boundary value problems for pulverized media with density hardening. Eng Trans 1971;19(1):15–42 [in Polish].
[57] Hueckel T, Mróz Z. Some boundary value problems for variable density materials. Problèmes de la Rhéologie. Warsaw: PWN; 1973. p. 173–91.
[58] Oda M, Iwashita K. Mechanics of granular materials. Rotterdam: Balkema; 1999.
[59] Bejan A. Heat transfer. New York: John Wiley & Sons; 1993.
[60] Schofield AN, Wroth CP. Critical state soil mechanics. London: McGraw-Hill; 1968.
[61] Hueckel T, Tao F, Cassiani G, Pellegrino A. Reactive plasticity for geological materials with a double structure evolving during aging. In: Picu RC, Krempl E, editors. Constitutive laws for engineering materials, fourth international conference, Troy, NY, 1999. p. 383–7.
[62] Bagi K. Stress and strain in granular assemblies. Mech Mater 1996;22:165–77.